



Review

Residual Stresses in Wire Arc Additive Manufacturing Products and Their Measurement Techniques: A Systematic Review

Fakada Dabalo Gurmesa 1,*, Hirpa Gelgele Lemu 2,*, Yosef Wakjira Adugna 2, and Mesfin Demise Harsibo 3,

- Faculty of Mechanical Engineering, Jimma Institute of Technology, Jimma University, Jimma P.O. Box 378, Ethiopia
- Department of Mechanical and Structural Engineering and Materials Science, Faculty of Science and Technology, University of Stavanger, N-4036 Stavanger, Norway; yosef.w.adugna@uis.no
- Department of Mechanicanical Engineering, College of Engineering and Technology, Wolkite University, Welkite P.O. Box 07, Ethiopia; mesfine2021@gmail.com
- * Correspondence: fd.gurmesa@stud.uis.no (F.D.G.); hirpa.g.lemu@uis.no (H.G.L.)

Abstract: This literature review provides an in-depth exploration of the research conducted on residual stresses (RS) in Wire Arc Additive Manufacturing (WAAM) products, particularly focusing on how process parameters influence the phenomenon. The motivation of the study is the growing focus on WAAM technology and the observation that RS plays a crucial role in determining the mechanical behavior and structural integrity of WAAM components. Thus, the review is intended to provide a better understanding of the relationship between process parameters and RS to optimize the WAAM process and ensure the durability of the final products. It also summarizes key findings, measurement techniques, challenges, and future directions in this evolving field. The review also analyzes measurement techniques used to characterize RS in products fabricated by WAAM as a function of process parameters. Experimental measuring techniques and numerical analysis of RS to determine the impacts of RS in mechanical responses in products of WAAM were discussed. Experimental measuring techniques, such as X-ray diffraction, neutron diffraction (ND), contour and ND, digital image correlation, thermomechanical coupling and contour, and hole-drilling methods, along with numerical simulations like finite element analysis, are discussed to determine the impacts of RS on the mechanical responses of WAAM products. Additionally, it addresses the influence of thermal cycles, cooling rates, and deposition strategies on RS formation. The role of material properties, such as thermal conductivity and expansion coefficients, in RS development is also considered. By offering a comprehensive overview of current research trends and insights, this review serves as a valuable resource to guide future investigations, fostering the advancement of WAAM as a robust and efficient manufacturing technology. The review also underscores the importance of interdisciplinary approaches combining experimental and numerical methods to tackle the complex issues of RS in WAAM, aiming to enhance the performance and reliability of additively manufactured components.

Keywords: residual stress; wire arc additive manufacturing; process parameters; residual stress measurement; wire arc additive manufacturing assessment



Citation: Gurmesa, F.D.; Lemu, H.G.; Adugna, Y.W.; Harsibo, M.D. Residual Stresses in Wire Arc Additive Manufacturing Products and Their Measurement Techniques: A Systematic Review. *Appl. Mech.* **2024**, *5*, 420–449. https://doi.org/10.3390/applmech5030025

Received: 27 April 2024 Revised: 15 June 2024 Accepted: 27 June 2024 Published: 10 July 2024



Copyright: © 2024 by the authors. Licensee MDPI, Basel, Switzerland. This article is an open access article distributed under the terms and conditions of the Creative Commons Attribution (CC BY) license (https://creativecommons.org/licenses/by/4.0/).

1. Introduction

Wire Arc Additive Manufacturing (WAAM) is an advanced manufacturing process that is categorized as additive manufacturing (AM) or 3D printing. It is the imperative metal manufacturing process for large and complex components, using wire metals or alloys as feedstock. In addition, due to its fast build-up rates, the metallurgical characteristics of WAAM fabricated parts, such as chemical composition and phase formation, are better than those of other AM techniques [1–3]. An important aspect that still hinders this technology is standardization and certification within nondestructive testing of the parts, which is discussed in the literature [4]. In this context, there are no standards for WAAM systems

and no in situ observing, and monitoring techniques for any instant formation of defects (residual stress) that can be fixed after its formation, which leads to waste materials and time for reproduction. WAAM is an innovative and versatile 3D printing technology with an extensive variety of applications and several advantages in manufacturing.

Early investigations suggest that the adoption of AM technologies in construction could potentially lower labor expenses, diminish material waste, and fabricate intricate custom shapes that typically challenge the manufacturer using conventional construction techniques [5–7]. However, the WAAM sector is interested in large-scale techniques with high deposition rates of AM for producing components, spanning from hundreds of millimeters to meters in size [8]. It harvests substantial attention in industrial manufacturing due to its cost-reliable fabrication of large-scale metal parts at high deposition rates [9]. Besides, Williams et al. [10] suggest that WAAM is a viable contender for substituting the existing manufacturing approach involving solid billets or extensive forgings, particularly for low to medium-complexity components.

Within the context of WAAM products, the presence of RS and deformations due to process parameters becomes a significant issue as they have a substantial impact on the quality, cost, and precision of the printing process [11–13]. Additionally, WAAM, which is a subset of AM, is getting significant interest from all researchers because of its various benefits, including its ability to achieve high metal deposition rates and produce near-net shapes, surpassing conventional manufacturing methods with its higher thermal residual stresses (RS) [3,14–16]. It is an emerging metal additive manufacturing technique that is gradually providing a competitive edge over traditional forging and casting methods [17]. Depending on the heat sources, the WAAM process is categorized into three, namely: inert gas welding, metal arc welding, and plasma arc [18,19].

The need and purpose of this review article is to investigate measurement techniques of RS in the products of WAAM. Notably, this review is essential to gain a deep comprehension of how RS is distributed in the products of WAAM and how it correlates with the deposition parameters. In this study, methods of examining and measuring RS, the impact of RS on the material characteristics of WAAM products, and process parameters based on both experimental and numerical analyses were discussed, while the mitigation of the RS and refining grain structure of created layer parts improved based on the experimental methods was discussed. In this review, the effects of process parameters like wire diameter, scan length with width, height (thickness) of bead, arc current behavior [20], voltage, travel speed, welding sequence (welding position) [21], types of shield gas, and its flow rate on RS are considered. Also, studies on the consequence of interlayer bead surface condition and inter pass time on the deposit shape and how it additively increased height were considered.

This review also primarily focuses on how to measure RS fabricated with WAAM, drawing upon pertinent data from the existing literature. The techniques for measuring RS through experimental approaches are mostly neutron diffraction [22–24] and X-ray diffraction (XRD) [25–27], which are performed within a limited layer depth of printed products, while the synchrotron-based X-ray can penetrate several millimeters into metals and alloys. Other methods like the hole-drilling strain-gauge method, ultrasonic stress measurement (USM), Barkhausen noise analysis, layer removal (deep-hole drilling), contour method, and incremental hole-drilling technique have been employed, and some of them have not been used yet. Importantly, this review explicitly delineates those that have been used and those that have not.

The format of the article is as follows: after this introductory section, Section 2 provides details about the materials and methods used in the research. This is followed by Sections 3 and 4, which, respectively, present an overview of the products of WAAM and discuss the impact of RS affecting the mechanical attributes of WAAM components. Section 5 focuses on explaining the mitigation strategies for RS and explores practical applications. Section 6 serves as a discussion section, offering a detailed analysis and

interpretation of the findings. Lastly, Section 7 summarizes the article by outlining the key points and providing insights into future research directions.

2. Materials and Methods

This review focuses on the scientific literature published within the last ten years, which encompasses sources primarily published between 2015 and 2024. This research is based upon the assessment structure of the PRISMA statement presented in Figure 1. To ensure comprehensive coverage of related research, the investigation targets the defects mainly on the RS of the WAAM products based on the many process and operational parameters. To achieve the aim of this review article, the review concentrates on the latest publications (as indicated based on the data given in Figure 2, with content thematically arranged around specific issues. The search was restricted to sources that have exclusively available articles published in English. It includes articles in the following scientific databases: scientific.net, Scopus, Elsevier, Science Direct, Web of Science, Compendia, Google Scholar, IEEE Xplore, ProQuest, ASM Digital Library, SpringerLink, Mendeley and ResearchGate, semantic scholar, SCISPACE, PubMed, DOAJ, JSTOR, MDPI, BASE, SAGE, Taylor and Francis, and others. It employed the English expression to search terms such as AM, WAAM, RS measurement, process parameters analysis, quality assessment in WAAM, WAAM product defects, characterization of microstructure in WAAM products, WAAM quality control, WAAM RS investigation, and frequently utilized additional descriptive terms to align with the review's objectives precisely. To accomplish this objective, these statistical combinations and analysis of data from multiple studies were used to draw overall conclusions.

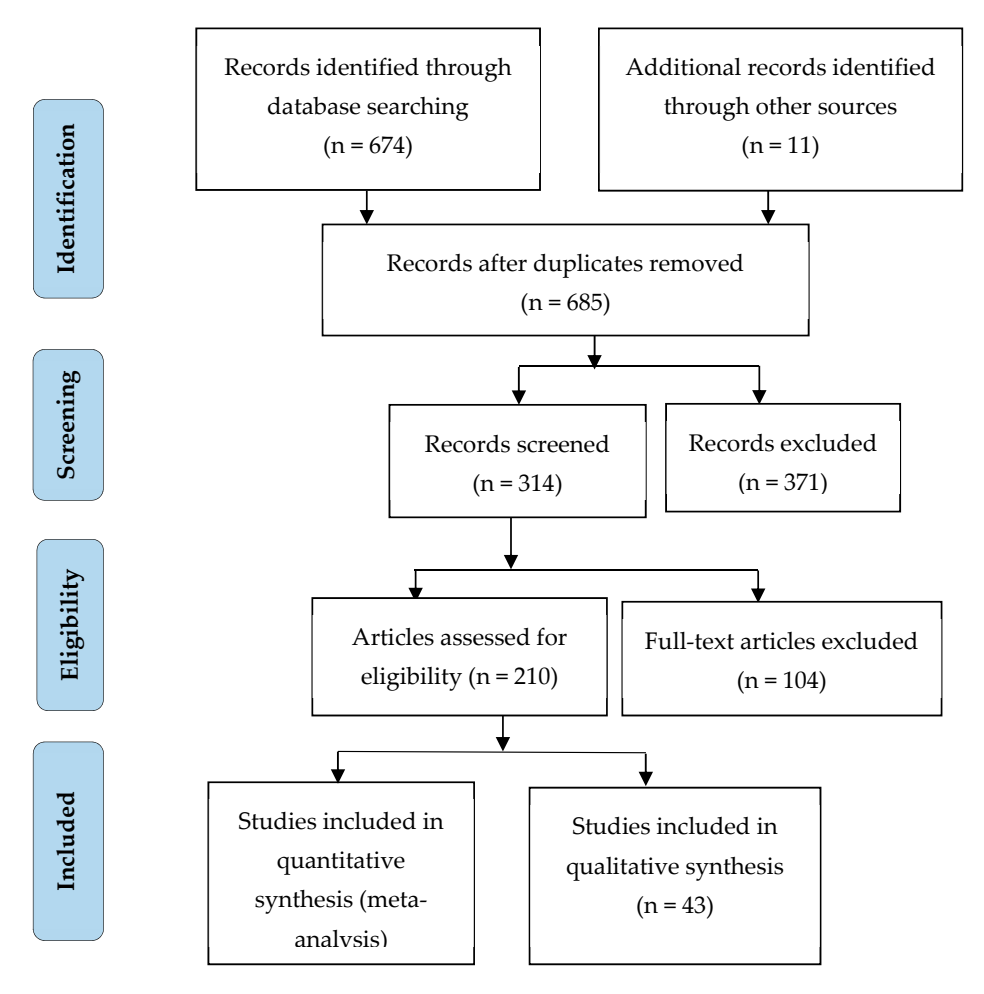


Figure 1. Flow diagram illustrating the screening and selection process of studies.

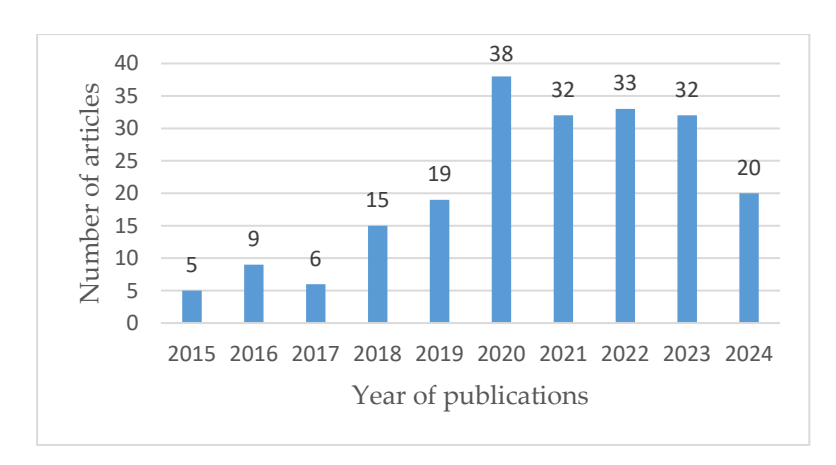


Figure 2. Statistical data on the reviewed articles of a Wire Arc Additive Manufacturing (WAAM) process publication from 2015 to 2024.

The assessed number of research fields of RS in WAAM is shown in Figure 2, depicting the yearly count of research publications. The bar graphs in the figure show that there has been a noticeable increase in research interest in RS in WAAM parts in the last few years, reflected by the rising number of publications in this domain. A high citation count usually indicates a high interest in the topic with the research community. For the chosen topic, the main strategy used to screen from the retrieved articles is 685, finally, the total number of articles that passed the screening (included in this article) is 209.

3. Overview of WAAM of Process and Products

In this technology, large and complex components are made from multiple material with a rapid deposition rate, a feat that is challenging to accomplish with traditional AM methods [28,29]. In this case, wire is supplied to the welding torch and melted by an electric arc [30]. Either robotic or computerized numerical control gantries are used to set the motion of the printing process layer by layer up to the aspired appearance of the components obtained [10]. The 3D digital model serves as the blueprint for this WAAM process. Utilizing robotic guidance in WAAM allows for a potent blend of automation and design flexibility, coupled with efficient production processes. However, the material characteristics response of wire arc additive manufactured (WAAMed) products is influenced by both automated robots and computerized numerical control to build up the parts and the associated heat input [31].

Basically, the steps used for the printing process in WAAM products encompass many activities in each stage, starting from the CAD model. These steps outline the general workflow for producing components using WAAM, ensuring efficient and reliable manufacturing of complex metal parts. The process of WAAM will be divided into six primary stages from CAD file preparation to component separation to post-processing [10]. The procedure planning steps used for WAAM to produce components are shown in Figure 3.

In essence, the RS is inherent in WAAM components due to the various process parameters that can adversely impact the mechanical properties, fatigue life, and structural integrity of the parts. Additionally, measuring RS in WAAM structures is challenging due to its time-consuming process, and because it lacks sufficient resolution [32]. The significance of understanding RS in WAAM products is critical for maintaining structural integrity to address premature failure and ensure the products' mechanical performance [18,33]. The characteristics of the deposited materials may vary through the WAAM process, affecting the evolution of RS [34], as a result of the heat-affected zone (HAZ) in the vicinity of the weld pool [35]. RS measuring also helps in understanding, predicting, and correcting dimensional inaccuracies caused by distortions, ensuring that WAAM products meet desired tolerances [36,37]. Likewise, accurate knowledge of RS is important to enhance product quality and ensure WAAM components meet their performance. By reducing the

risk of defects, failures, rework, and/or remanufacture, it can lower production costs and minimize material waste [36,38,39].

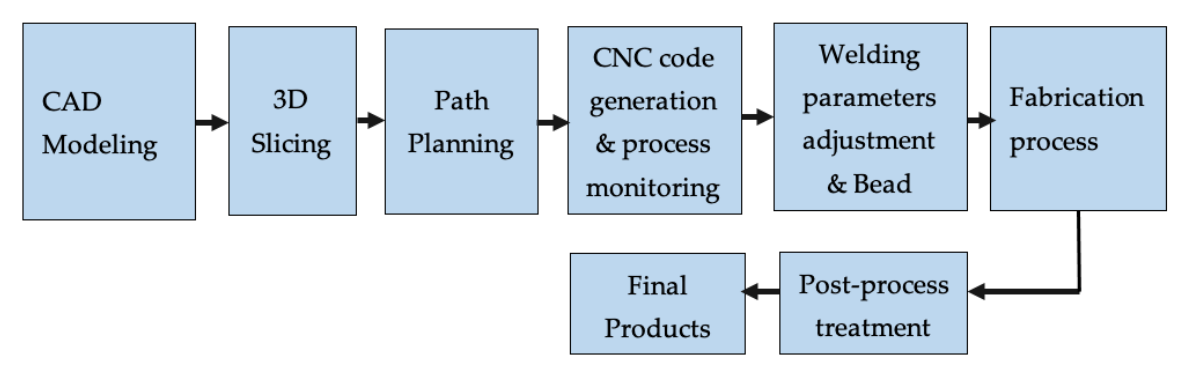


Figure 3. Steps used for WAAM to produce components.

WAAM can be utilized for repairing and restoring damaged or worn components and extending the lifespan of expensive equipment and machinery [40,41]. Furthermore, it is highly capable of building large and/or complex, cost-effective metal structures, primarily as a result of its superior deposition rate [3,7,30,42–47]. WAAM is well-suited for creating sizable metallic parts and holds potential for use in the construction industry among various AM methods [20]. The main advantages of these manufacturing methods include their productivity, suitability for industrial applications, and the capacity to decrease material waste compared to other AM techniques [48,49].

3.1. A Robotic System for WAAM

Robotic systems play an important role in WAAM processes, providing versatility and automation that enable precise control over deposition parameters and the capacity to manage intricate geometries [50,51]. These systems incorporate advanced sensors and automation technology to monitor and adjust printing parameters in real time, ensuring consistent quality and the precise deposition of materials. The study reported in [52] concentrated on two WAAM parameters, namely (1) the speed of wire feed and (2) the robot's movement speed, and investigated their effects on the metallurgical, dimensional stability, and mechanical characteristics of materials. The study involved the production of fine-walled 308L stainless-steel parts utilizing the WAAM system, conducted in two steps. Firstly, the effect of welding current, voltage, and travel speed on the shape of individual weld beads was examined, and these factors were fine-tuned for the construction of 308L steel walls. Secondly, a comprehensive analysis was conducted on the influence of the microstructure and mechanical characteristics of the WAAM 308L steel walls, resulting in improved mechanical properties suitable for industrial applications. Robotic components for the printing process with the path of indentation (Figure 4a), the setup for experimentation (Figure 4b), and the deposition tool path are illustrated in Figure 4.

Genetic Algorithms (GAs) are used to enhance the parameter selection process in near-net shape deposition for minimizing voids and surplus substances in the WAAM process [53]. An uninterrupted deposition process is planned by verifying overlapping conditions within robot swap zones to avoid collisions [54,55]. Likewise, a continuous deposition process is being planned carefully by checking areas where robots might overlap or come close to each other in robot swap zones. This careful planning is done to prevent any collisions between the robots, ensuring smooth and safe operations. The robotic guidance will be fixed on the desired welding speed, which affects the heat accumulation and results in variations of the RS in the products, as well as the robotic guidance to monitor the process in the WAAM described in Figure 4. Employing path planning was proposed [53,54] to incorporate bead overlap and enhance internal structural stability by minimizing height; eventually, it influences the RS in WAAM products.

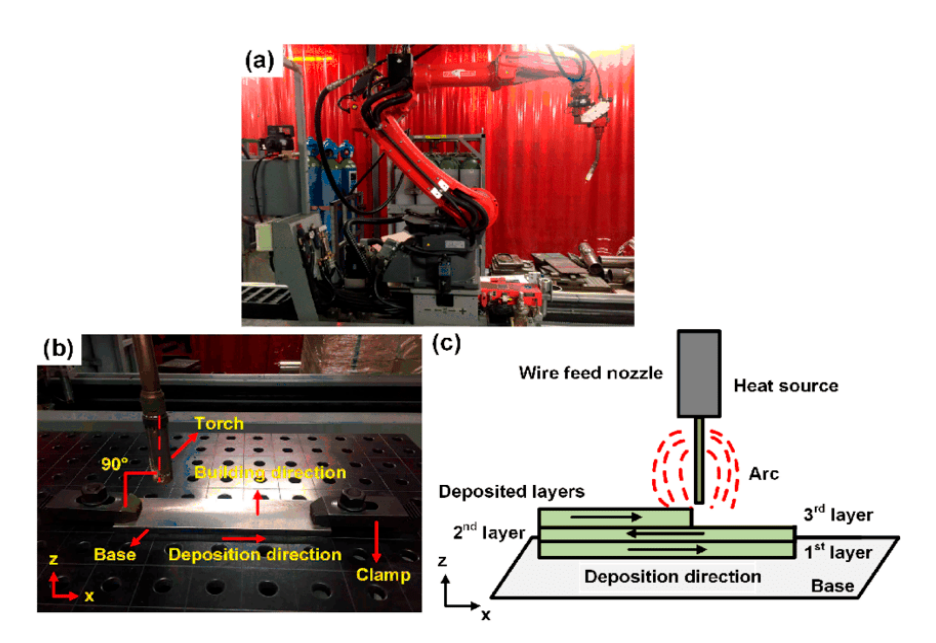


Figure 4. (a) Configuration of robotic WAAM system, (b) setup for experimentation, (c) deposition tool path [53]. Copyright 2019. MDPI, in accordance with CC BY license, open access.

3.2. Residual Stress in WAAMed Products

RS in WAAM refers to the internal stresses that remain locked inside a part (thermal RS) within fabricated components [55]. When a component within this RS is subjected to cyclic loading or stress, it can accelerate the initiation and propagation of the cracks, which is the reason for premature failure [56]. This RS may arise from various factors, such as the cycles of heating and cooling associated with the differential expansion during the welding process, contraction of materials during cooling time, and other process parameters [57–62]. Ahsan et al. [63] identified that the high heat input is a near-optimal processing condition to improve surface quality, ductility, and deposition rates due to the induced high RS. In the WAAM process, the component will induce heat tension and thermal distortion as temperatures fluctuate with the advancement of fabrication [64,65]. This adjustment is made by controlling the values of wire-feeding rates and travel speed (TS). With higher heat input, the lower RS is observed on the surface of the top layer by long-time cooling durations [66]. Welding RS was measured using five experimental methods: X-ray diffraction (XRD), neutron diffraction (ND), incremental deep-hole drilling (iDHD), incremental center-hole drilling (iCHD), and the contour method (CM) [67].

As researchers delve deeper into WAAM, they have discovered significant enhancements inside the grain arrangement and material properties of the produced components [68]. The transformation of large, elongated grains into smaller, uniformly shaped grains in both the inner and intermediate layers is accomplished by adjusting the amount of heat applied [65,66]. The influence of heat input on the RS, macroscopic structure, microscopic composition, and mechanical characteristics of the components fabricated through the WAAM procedure is studied in [69,70].

3.3. Residual Stress-Measurement Methods

Compared with measuring RS in other conventional methods, measuring RS in WAAM products is more challenging due to the complex thermal history, microstructural heterogeneity, geometric complexity, and the need for specialized measurement techniques. Addressing these challenges requires a combination of advanced experimental methods, accurate calibration standards, and robust modeling and simulation tools. Understanding and overcoming these challenges is critical for ensuring the structural integrity and performance of WAAM components in practical applications. Generally, there are two measuring techniques of RS for WAAM-fabricated parts, namely experimental and numerical methods, which are reviewed and reported in the following subsections.

3.3.1. Experimental Methods for RS Measurement in WAAM Parts

Several review articles across different literature types have investigated the examination of RS in WAAM products using various techniques [71]. Initially, these studies focused on the stress in the central lines of the cross-section of the general beam theory, conducting a theoretical analysis of stress evolution along these lines without assuming a specific stress distribution, which is considered RS. Subsequently, the research expanded to improving forecast models for warpage based on general beam theory [72]. Other techniques encompass neutron diffraction (ND) [22–24,73], X-ray diffraction (XRD) [25–27,74], the contour method [13,75–77], hole-drilling methods [31], the thermomechanical coupling model [78], digital image correlation (DIC) [79], deep-hole drilling (DHD) [80], Operando synchrotron, and synchrotron X-ray diffraction (SXRD) [81,82]. The selection of the methods depends on elements such as material, component size, geometry, and the level of accuracy required for the measurement. An accurate modeling of the process is crucial for understanding and controlling RS. For instance, XRD analysis is utilized to identify the grain size observed in the thin strips and ferrite of bainite created due to thermal cycles, while dye-penetration tests are used to investigate surface defects and corrosion behaviors of WAAM components [65,66,68,83].

The choice of the appropriate measurement method is governed by factors such as accessibility, resolution, accuracy, and the desired depth of stress penetration. Table 1 lists the methods used for RS measurement on different materials together with the summary of the experimental studies. As can be observed from the table, the most used methods, according to the literature overview, are XRD, ND, digital image correlation (DIC), SXRD, layer removal (deep-hole drilling), the contour method, and the incremental hole-drilling method.

Table 1. Summary	v of experimenta	l methods for residua	1 stresses (RS) measurement.

Methods	Materials	Results	Refs.
ND	316L stainless steel	The process parameters' influence on RS is barely noticeable in the melted zone.	[22]
	Fe3Al alloy	Large columnar grains result in anisotropy and RS is tensile in the building direction, and the tension to compression progressively moves up from the beginning to the end of the deposition way.	[23]
	AA6061	RS indicates the occurrence of tensile stresses with a greater magnitude in the constructed parts, while the substrate exhibits fewer compressive stresses. No significant dissimilarities were seen in mechanical properties.	[59]
	2319 aluminum alloy	RS along the build direction in the deposited wall is tensile stress, extending up to the floor. The inter-pass rolled walls reduced RS to enhanced strength in the longitudinal direction.	[24]
	Fe3Al	RS and distortions resulting from the WAAM process are major concerns as they not only influence the part tolerance but can also cause premature failure in the final component during service.	[83]
	stainless steel 304L	The alteration of RS in the specimen after introducing a new deposit. Longitudinal stress was predominantly tensile, reaching its peak at the boundary between the parent material and the layers where the thermal loads were applied.	[84]
	Inconel 625	Measurements showed that lower RS formed in the direct interface functionally graded materials (FGM) compared to the smooth gradient FGM.	[85]
Contour and ND	Ti-6Al-4V alloy, stainless steel	The stress in the baseplate varies RS. The lattice parameters were not valid in the baseplate for ND measurements. Cutting out a stress-free exit was used to correct reference samples.	[73,74,86]

Table 1. Cont.

Methods	Materials	Results	Refs.
XRD I	Alloy C-276	The amplitude of tensile RS was perceived in the travel direction compared to the build orientation. The residual strain in the lattice reveals the RS in the material. The larger amplitude of compressive RS was found in the build axis.	[87]
	Al-5356 alloy	The height of the beam can impact both the level and pattern of longitudinal RS in both the substrate and the beam. This variation primarily affects transverse RS in the substrate and has minimal influence on the beam itself.	[88]
	G 79 5 M21 Mn4Ni1.5CrMo (EN ISO 16834-A) [89]	RS, hardness, and microstructure are influenced by welding parameters, geometry, and component design. Heat input causes decreased tensile RS, which causes unfavorable grain structure and mechanical response.	[25]
	SS308L austenitic stainless steel (SS)	Accumulation of compressive RS attributed to elevated heat input and rapid cooling rates. Greater stress happened closer to the welding base than in other areas.	[26]
	Al-6Cu-Mn alloy	The advancement of RS indicates that the most crucial area of the sample is near the substrate, where significant tensile stresses near the material's yield strength are dominant.	[27]
-	Grade 91 (modified 9Cr–1Mo) -steel	RS varies the characteristics of the material and its microscopic structure WAAMed ferritic/martensitic (FM). The heat treatment applied to the originally manufactured steel did not remove its anisotropic properties.	[80]
	Inconel 625	Post-treatment heat processes can enhance corrosion resistance and alleviate RS. Measurements indicated that the smooth-gradient approach produced secondary phases like d-phase (Ni3Nb) and carbides, which were absent in the direct interface method.	[85,90]
DIC	Mild steel (AWS ER70S-6)	DIC was employed to oversee the flexural distortion of WAAM components while being released from the clamped H-profiles, and residual tensions were deduced from the strain distribution observed during the unclamping process.	[77,91]
Deep hole drilling	Mild steel (G3Si1) & austenitic SS (SS304)	RSs are under compression in the mild steel section and under tension in the austenitic stainless steel (SS) section. These stresses fluctuate across the thickness because of differences in cooling rates on the interior and exterior surfaces.	[78]
Hole drilling	Ti-6Al-4V	Grain size decreased after ultrasonic impact therapy and RS of fabricated parts in WAAM after post-UIT are improved.	[76,92]
Thermomechanical coupling & Contour	Stainless steels (SS) SUS308LSi	RS is tensile in the layers bordering the surface's upper surface, compressive in the layers near the substrate surface, and tensile near the underside of the substrate.	[13]

The RS measurement techniques listed in Table 1 can generally be classified into three categories: (1) non-destructive; (2) semi-destructive; and (3) destructive are mentioned in Table 1 with short descriptions, while some of the techniques were not performed in the past research. Non-destructive techniques (NDT) like XRD and ND are common high-precision methods and are frequently preferred to measure RS in WAAM components. The choice of the methods depends on fundamentals such as material, component size, geometry, and the level of accuracy required for the measurement.

It is clear that from RS measurement techniques, ND has been utilized more extensively by researchers due to its non-destructive nature, which helps maintain the veracity of the parts, while X-ray diffraction is the second method utilized. The pie chart shown in Figure 5 represents the hierarchies of techniques used to measure RS in WAAM products. The elastic strain in RS is calculated from the change in the lattice spacing [23]. In this case, any stress,

whether external or residual within a material, leads to deformation and changes in lattice spacing. Stress is determined by measuring lattice distance at different tilt angles using Bragg's law, which explains X-ray diffraction in crystal lattice planes. From several NDTs for identifying RS, XRD was mostly selected due to its capability to penetrate approximately $10~\mu m$ and provide spatial resolution ranging from $10~\mu m$ to 1~mm, rendering it particularly suitable for thin-plate applications [26].

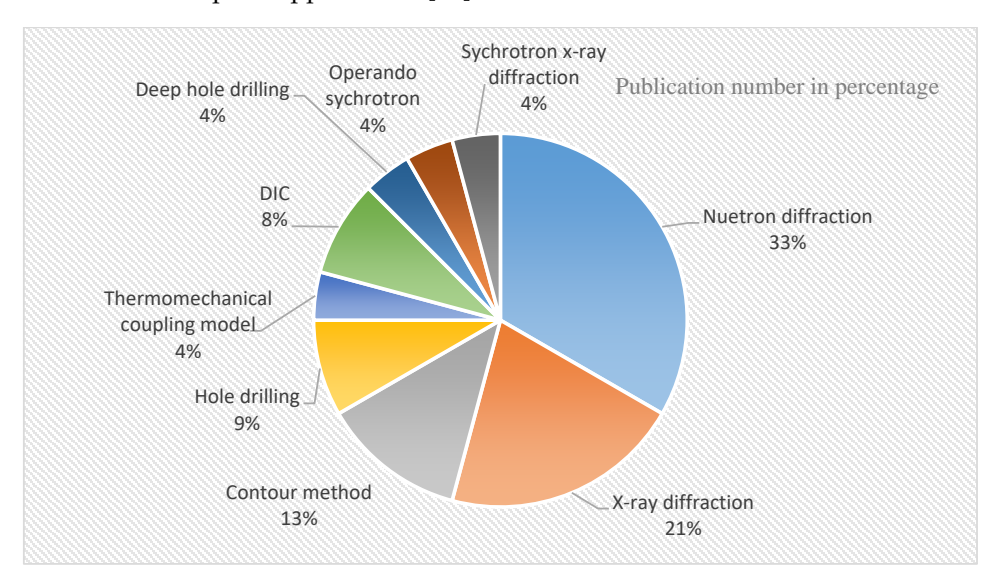


Figure 5. Pie chart research field distribution sorted based on the quantity of RS.

3.3.2. Numerical Analysis of RS in WAAM Products

Behind the numerical analysis of RS, there are mathematical models often based on finite element analysis (FEA) or other computational methods, and the same procedures are performed to determine RS in the WAAM process for simulating thermal and mechanical processes occurring during AM. These models incorporate material properties, process parameters [68], and boundary conditions to simulate the deposition, while heat-measurement techniques mention the highest proportion and/or the lowest proportion transfer, as well as subsequent cooling processes. By solving governing equations for heat transfer, numerical simulations predict the evolution of RS within the part. Similarly, the numerical analyses examine how deposition patterns and travel speed affect RS and warpage in WAAM components [93]. Table 2 provides overviews of the numerical analysis techniques, feedstock materials, and their outcomes when utilized in the WAAM process.

Table 2. Overview of reported numerical analysis using finite element method (FEM), tools, and materials related to WAAM technologies.

FEM Softwares	Material	Summary	Ref.
ANSYS 2019	B91 steel (ER90S-B91 steel)	A thermomechanical assessment of WAAM B91 steel was performed sequentially to assess the variation in residual stress throughout the component.	[11]
Simufact Additive 2023.2	Steels	The dynamic temperature changes, alteration, stress accumulation, and deformation hold significant importance for applications involving high-strength steels.	[40]
ABAQUS 2019	Aluminum alloy	Deposition pattern and travel speed have an impact on RS and warpage in WAAM parts. Results of thermomechanical FE simulations show that the out–in deposition pattern leads to the highest levels of RS and warpage. Increasing travel speed lowers peak temperature and thermal gradient in deposition, reducing RS.	[94]

Table 2. Cont.

FEM Softwares	Material	Summary	Ref.
	Inconel 718	Utilized a comprehensive 3D transient heat-transfer model to calculate the temperature distribution and gradient in the WAAM process for various process parameters, which results in RS. The derived temperature data were utilized in a mechanical model to forecast RS and distortion.	[95]
	Carbon steel	The modeling outcomes indicate that as the count of deposited layers rises, the maximum temperature rises, resulting in RS, while the average cooling rate decreases.	[96]
ABAQUS 2010	Austenitic stainless steel (304) and low Carbon steel (A36)	By systematically altering one mechanical property at a time, we isolated the influence of each on RS formation in dissimilar welds. Results show that longitudinal residual stress in both alike and different welds can be diminished within the weld zone by an amount equivalent to the stress caused by applied mechanical tensile force once the tensioning force is released post-cooling.	[97]
API X65 steel Structural steel ER70S-6 wire	API X65 steel	Thermal conditions and RS are forecasted precisely to allow for the regulation of the fusion zone's shape, microstructure, and mechanical characteristics in the Submerged Arc Welding joint.	[98]
ABAQUS 2019		The residual stress and deformation of two extensive builds were examined, revealing highly consistent numerical findings and favorable correspondence with experimental outcomes.	[99]
	EH36 steel	The effect of the scanning speed on thermal profiles and RS indicates that higher scan speeds result in reduced peak temperatures and heightened cooling rates, thus leading to a rise in the volume portion of martensite within the deposition.	[100]
	Aluminum alloy	The RS and deformation were computed using the moving heat sources (MHS) method and the segmented temperature function (STF) method.	[101]
	Ti-6Al-4V, S355JR steel & AA2319	Reduced profile radii of roller effectively eliminate almost all tensile RS near the surfaces.	[32]
MSC. Marc 2021	Y309L	Elevated RS is generated within the deposition layers and also within the middle of the substrate.	[102]
MSC. Marc 2014.2.0	Welding filler G3Si1	Simulation and validation regarding geometry and microstructure variations within the welding passes were conducted with RS reality and simulation using measurement inertia of the thermocouples.	[103]
	S316L	The variances in RS are influenced by both the fluctuating temperature distribution during the freezing phase and the forces applied to the WAAM structure following the cooling process.	[104]
COMSOL-5.4 2018	304 Stainless steel	Large-scale images and high-speed recordings were used for the wall constructed to verify the accuracy of the measurements of the molten pool and the form of the deposition determined, which decided the RS in parts.	[105]

Drexler et al. [106] addressed the numerical modeling of RS and distortions occurring in WAAM parts with weaving deposition. Numerically forecasted thermal stresses across various welding layers were depicted for subsequent experimental evaluation conducted in [107]. Similarly, finite element (FE) simulation, along with thermal analysis, generated appropriate paths by segmenting a 3D surface scan of the intended repair area [41]. As illustrated in the pie chart in Figure 6. (ref. also Table 2), most of the numerical analysis of RS was investigated using ABUQAS 2010 and 2019.

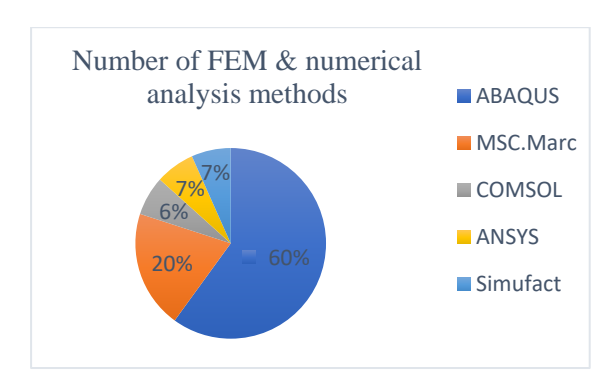


Figure 6. Quantity of publications on FEM used for RS in WAAM process published with some materials.

3.4. Factors Influencing RS in WAAM

Researchers and engineers can characterize and understand the RS behavior in WAAM components by employing experimental methods and Finite Element Analysis (FEA), leading to improved process control, part quality, and product performance. Many parameters that can influence RS in WAAM parts are discussed in [18], while a profile that includes an assessment of the overall height, width, and smoothness of each generated wall was studied and reported in [108]. Deposition parameters [109], heat input, interlayer temperature, and the duration of interlayer pauses were significant factors influencing the formation and distribution of pores in aluminum 5183 alloys printed in the WAAM process [110]. Similarly, different welding travel speeds at which defects become noticeable also imply both wire-feed speed and travel speed in the welding process [111]. In contrast, substrate (bed or baseplate) thickness was found to have a major influence on the RS distribution along deposit height. Due to the substrate, tensile RS as high as the value of the material yield strength was discussed in [112]. The RS distributions in both the longitudinal and transverse directions indicate that longitudinal stress shifts significantly from compression during the deposition to tension in the baseplate [113].

Moreover, a thicker substrate induces greater RS than a thinner substrate. A substrate that is used for molten pool dropped on (printing process) can be made of a $2\times\times\times$ aluminum alloy plate for aluminum alloy feedstock [114,115]. In the direct 3D printing process, the position of the printed sample matters to the quality of the printed parts [64]. This is because the expansion of isotherms fails to reach the bottom of a thick plate, resulting in increased heat accumulation [116,117]. The technique controlling inherent RS and distortions faces numerous challenges in the WAAM products, leading to unpredictable structural integrity in the printed parts. For such reason, some literature identifies that different process parameters like wire-feed rate, travel speed, heat input, deposited path length, width, and depth (thickness) of printed components have effects [46,55,118]. The main defects induced in metal-manufacturing components due to these parameters in the WAAM process identified by many investigators are RS, deformity, porosity, cracks, and distortion. Thus, the most common factors of WAAM products' defects are the process parameters, which limit the acceptance of this technology [119–123]. In another way, undercut and humping are the common defects found in the WAAM products, while the major influences of deposition height, width, and stable layer produce heat input per length values [111].

The processing condition effects, such as interlayer temperature, deposit height, and substrate thickness on the distribution and magnitude of RS, were studied in the literature [112,124,125]. The majority of substrates revealed the rewarding compressive RS, while the deposit beads showed tensile stress. The instrument of absolute distance measurements is incorporated into the WAAM system to deliver monitoring processes of deposit layer height, profile, and bead volume predictions during the processes. Micrometers by handand laser-scanning measurements were also used after each completed deposit [126,127]. WAAM encompasses a multitude of adjustable process parameters, such as wire-feed rate,

voltage, current, travel speed, and layer height [128]. These parameters govern various aspects of the deposition process, including heat input, cooling rate, and thermal gradients. Understanding how alterations in these parameters influence RS is vital for achieving optimal WAAM product performances [111]. The selection of bead geometry parameters in the WAAM process is required to optimize excess materials and minimize the void created in the multiple layers of bead depositions. Process parameters and other factors influencing RS in WAAM components are summarized and listed in Table 3.

Table 3. Factors influencing RS in the wire arc additive manufacturing.

Process Parameters and Other Factors	Short Description	Refs.
Material properties: weldability of the materials	Not all materials are equally suitable for WAAM. The process often requires materials with good weldability characteristics, such as low susceptibility to cracking and good fusion properties. For instance, materials' thermal conductivity, coefficient of thermal expansion, and phase transformations can impact RS induced.	[13,34,129,130]
Deposition power: Arc current & voltage	In the WAAM process, controlling the heat input is critical to prevent overheating, distortion, and metallurgical issues, such as excessive grain growth or phase transformations. Variations in heat input alter materials' weldability consequences of RS.	[25,65,66,114,130,131]
Speed: wire feed speed, welding travel speed, and deposition rate	Rapid deposition and cooling can lead to increased RS, especially near the deposition zone. The rapid solidification and higher deposition rate can cause thermal gradients and differential cooling rates, resulting in higher levels of tensile RS. Increasing the welding travel speed reduces the amount of time the material spends in the high-temperature zone and leads to the lowering of the magnitude of RS.	[113,132–134]
Shielding gas: types of shielding gas, and shielding gas flow rate	Shielding gas plays a crucial role in WAAM processes as it protects the molten weld pool from atmospheric contamination and influences the heat-transfer characteristics during deposition. The type of shielding gas, gas-flow rates such as argon and helium, and reactive gases like CO_2 and O_2 can have significant effects on RS formation in WAAM products.	[3,37,135]
Nozzle distance: Nozzle tip to work distance (Welding torch distances)	The welding torch distance in WAAM processes can have a significant influence on RS in the final products. Optimizing the nozzle tip to work distance in WAAM processes involves balancing the heat input, cooling rates, distortion control, interlayer bonding, and defect formation to minimize RS and ensure the production of high-quality parts.	[23,24]
Printing position: Electrode to layer angle (wire) (θ) and layer height	The printing position affects heat dissipation and buildup, influencing the cooling rate and thermal gradients within the part. The printing position affects the flow of molten metal and the geometry of the deposited beads results in variation of RS.	[36,64,128,136,137]
Layer thickness: Substrate thickness, deposition thickness	Decreasing the layer thickness in WAAM fabrication can lead to shorter thermal cycles and reduced heat input per layer. This may result in lower overall RS due to less thermal distortion and reduced HAZ size.	[124,138]
Cooling rate: Deposition of layer time, dwell time between layers	e, dwell time structural integrity and dimensional accuracy of the components, making it challenging to	
Preheating substrate (Baseplate)		
Part geometry: Printed part shapes & volume of the parts		
Post-Weld Heat Treatment (PWHT)	PWHT plays a crucial role in managing RS in WAAM products. By subjecting the parts to controlled heating and cooling cycles, PWHT can effectively alleviate RS, improve material properties, and enhance the overall quality and implementation of the manufactured parts.	[1,4,60,112,139]
Scanning pattern	The scanning pattern plays a crucial role in influencing heat accumulation, cooling rates during AM deposition, and, consequently, the formation of RS.	[100]
Wire filler: wire filler diameters and wire grade	The filler wire diameter and wire grade are two key factors that can significantly influence RS in WAAM products.	Not studied

The height of the bead, width, and cross-sectional area of the beads are expressed using the process parameters [140]. Furthermore, the diameter of the wire is expected to significantly influence both the melting efficiency of the wire and the mode of metal transfer, which are crucial factors in enhancing the deposition rate of WAAM. Nonetheless, the comprehensive effects of wire size on process attributes and deposition rate in plasma transfer arc-based WAAM remain inadequately comprehended. The primary objective is to examine the optimal combination of wire diameter with the Wire Feed Speed (WFS) to achieve higher deposition rates and improved bead geometry while also addressing process-control challenges and defect avoidance at elevated deposition rates. All aspects of the limitation of the deposition rate, bead-shape control, keyhole formation, and metal transfer are studied in [42]. The selection of welding parameters in the WAAM is investigated in [141], and the values of the range used are explained in [142]. In the pie chart diagram in Figure 7, the factors that influence the residual stress in WAAM parts are plotted in percentages.

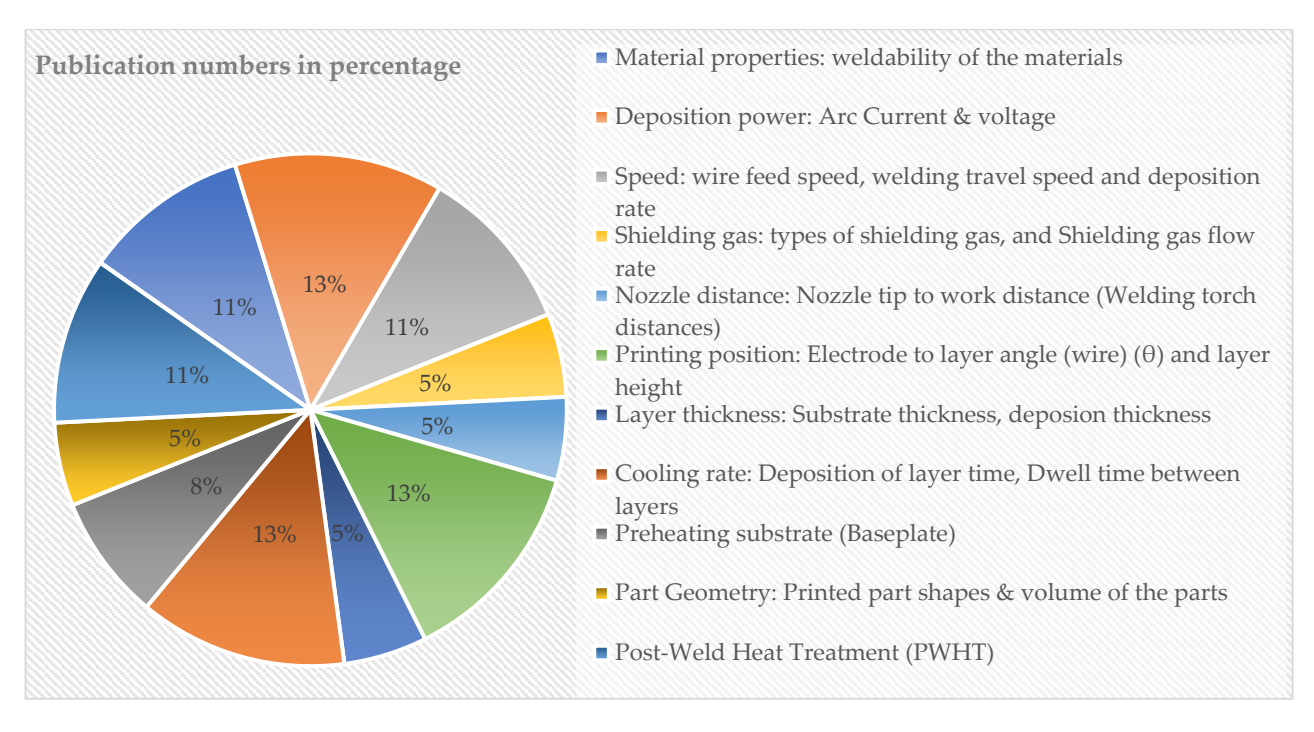


Figure 7. Pie chart of research field distribution sorted based on the number of factors influencing RS.

The elevation of the bead grows in a nearly proportional manner with the rise in the wire-feed rate, while the width of the bead decreases only at the subsequent feed rate. Moving on to the travel speed, it is observed that the width of the bead diminishes as the travel speed increases, whereas the bead height remains relatively constant. Furthermore, the wetting angle decreases as the travel speed increases [143]. The explanation of computing heat input per unit volume is outlined. The research indicated inconsistencies among various standards in interpreting heat input. Furthermore, the practical implementation of the method for calculating the precise heat input into the weld was validated [132]. Naveen et al. [144] conducted research by focusing on process parameters effects on products made of 5356 aluminum alloy on WAAM with three parameters, namely: (1) wire-feed rate, (2) welding speed, and (3) gas-flow rate of value product of weld beads. The technique adopted was the Taguchi method to decrease the trial number for choosing a range of input variables. Successful efforts have been made to optimize welding modes for the WAAM applications in which more grain microstructure is studied [145].

The Taguchi technique, along with ANOVA, was employed to analyze how travel speed, wire-feed rate, current, and argon flow rate impact various outcomes such as bead shape and size, bead roughness, oxidation levels, melt-through depth, and microstructural

characteristics [143]. Based on the energy-dissipation hypothesis and associated equations, various additive manufacturing processes utilizing energy beams can be compared more thoroughly when subjected to equal energy input. This comparison serves as a foundation for determining the initial process parameters and the dynamic adjustment of the main parameters [146]. The amount of heat input generated in the welding arc per unit length of the weld is expressed in kilo Joules per millimeter length of the weld (kJ/mm), as shown in Equation (1).

$$Arc energy (kJ/mm) = Volts \times Amps = V \times I$$
 (1)

where V is in volts and I is in ampere (A). The amount of heat input generated in the welding arc per unit length of the welding process is represented in Equation (2), and in different ways as per the ASME IX QW-409.1 standard from the American Society of Mechanical Engineers [132].

Heat Input(J/mm) =
$$\frac{\text{Volt} \times \text{Amps} \times 60}{\text{Travel Speed (mm/min)}} = \frac{V \times A}{v}$$
 (2)

where v is the travel speed. Vora et al. [147] investigated that voltage had the greatest influence on bead width, followed by travel speed and the ratio of gas mixture.

The deposited layer during the fabrication process for bead formation is assumed to be semi-circular. The deposition rate, R, which is influenced by wire diameter, wire-feed speed, and wire density is expressed as Equation (3).

$$R = \frac{\pi d^2 v \rho}{4} = \rho v A_{ww} \tag{3}$$

where d is the wire diameter, v is the wire-feed speed (WFS), and ρ is the wire density and A_{ww} welding wire cross-section area.

4. Impact of RS on Mechanical Properties in WAAM Components

Although WAAM has shown its capability to produce medium-to-large-sized components from aluminum for automotive and related industries, it cannot yet serve as a comprehensive production method due to practical challenges such as unmatched mechanical properties and significant RS [148]. RS significantly affects the materials and mechanical characteristics of the manufactured component. For instance, it can affect the mechanical properties, such as the strength, hardness, and ductility of products, by making them different from the material's intrinsic properties. High heat supply in the WAAM process results in reduced tensile stress within the component and can lead to undesirable mechanical properties and microstructure [149,150].

Microstructural characteristics have an impact on the material properties of WAAM fabricated products, including the residual stress levels. The microstructure of WAAM products plays a critical role in the development and distribution of RS, which affects the many interrelated mechanical properties. Due to the existence of RS in WAAM products caused by the rise in either welding speed or the heat-distribution parameter, material properties can be significantly varied [103,151]. The resultant microstructure and RS level in WAAM are directly correlated with the ultimate mechanical properties. Research on internal porosity in beads formed and its capability to produce large-scale components demonstrates inadequate tensile and fatigue properties [152]. This porosity is a result of RS by affecting the solidification process and the ability of gas to escape during deposition [153,154]. Similarly, RS can influence various mechanical properties of the manufactured parts in several ways by changing strength, toughness, microstructure, fatigue life, cracking, and delamination of the WAAM products [152,155].

RS formed during the fabrication process markedly impacts mechanical performance and may result in detachment from support structures, undesired shape deformation, and premature crack initiation [76]. The input parameters, resultant microstructure, postmanufacturing treatments, and RS have significant impacts on the ultimate mechanical

characteristics of WAAM products [1,156,157]. The accuracy of the formation of the deposition layer is influenced not only by the precision of the arc torch's positioning but also by the stability of the forming process [158].

Figure 8 depicts the challenges and inherent RS in WAAM parts where reheated and remelted parts are the known phenomena in high technology during the manufacturing process. To achieve good grain structure in each layer, the minimum penetration depth of plastic strain should exceed the sum of the remelting depth and the height of the newly deposited layer. To enhance the microstructure, the minimum depth of plastic strain must exceed the combined depth of remelting and the height of the newly deposited layer [32].

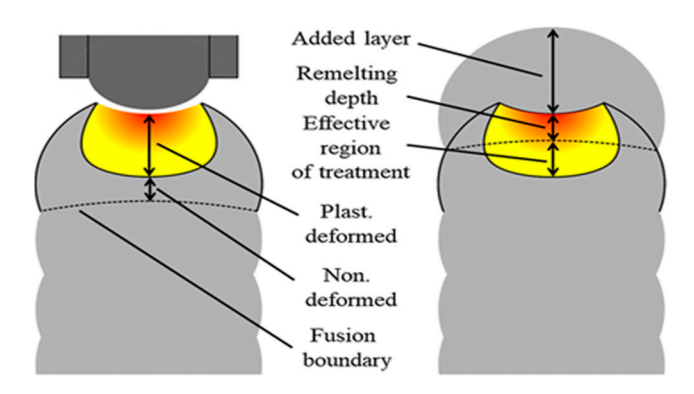


Figure 8. Diagram illustrating the remelting phenomenon occurring during the deposition process [32]. Copyright 2019, in accordance with CC BY license, open access.

The experiments for the investigation of RS were conducted on the WAAM-based products by using cladding of single beads using welding voltage and current parameters as variables. The dependence of the formation of beads on the number of short circuits per unit length is explained in [49]. Even though the WAAM technology is an energy-efficient manufacturing method for metal production, heat accumulations during deposition, metal-lurgical, and associated mechanical property results can change the RS profiles across the cross-section of the fabricated components [11,13,159]. The impact of build orientation and heat-treatment schedule on the microstructure and mechanical properties of thin-walled components was examined in [160]. The distributions of RS within the component along the deposition path, both internally and externally, are equal to zero [161,162].

Overall, understanding and controlling RS are essential for ensuring the mechanical reliability, dimensional accuracy, and functional performance of WAAM products in various applications. Many research efforts focused on characterizing RS, developing predictive models, and implementing advanced manufacturing techniques, which are critical for advancing the field of WAAM and unlocking its full potential in industrial applications [100]. Comprehending the distribution of heat input and its implications, including transient temperature distribution, material transformation, stress accumulation, and distortion, holds significant relevance for applications involving high-strength steels. Numerical simulation can offer valuable insights for assessing these factors [40]. The RS and deformation significantly impact the performance of the components [97]. As a result of repetitive cycles, RS becomes confined within the components, causing an array of defects such as cracks, deformations, warping, and diminished component lifespan [163].

5. Mitigation Strategies for RS in WAAM and Practical Applications

The generation of RS and distortion in parts impedes its broad adoption due to the intricate thermal build-up histories characteristic of WAAM components [164]. However, mitigation strategies for RS in various manufacturing processes in WAAM involve several techniques to reduce or manage the RS that can impact the reliability and functionality of manufactured components. A hybrid process of WAAM and high-pressure rolling able to build large-scale components produces low detrimental RS and distortion [165,166]. In the same way, numerical methods can offer an additional understanding of how rolling can be

effectively utilized to diminish RS and generate the necessary plastic strains to enhance microstructural properties [32]. Combining the WAAM process with other fabrication processes, including machining or subtractive techniques, can assist in removing excess material. This hybrid manufacturing is used in the medical device industry to produce low-stress WAAM parts with complex geometries or add complementary features to reduce RS [167].

Controlling RS is vital for ensuring the durability and reliability of these critical components [130]. A compilation of different methods for mitigating RS and distortion in WAAM has been assembled to offer a blueprint for future advancements [168]. Finite element-process simulation offers an effective method to explore strategies to mitigate these distortions and RS [169]. Some methods provided techniques to handle RS, enhance mechanical properties, and eliminate defects like porosity [10,170]. Some common mitigation strategies and practical applications are listed and explained with practical applications in Table 4.

Table 4. Mitigation strategies for RS and practical applications.

Methods	Material and Strategies	Practical Applications and Results	Refs.
Inter pass rolling	Ti-6Al-4V alloy	Enhances the bonding and adhesion between the successive layers of material. It also helps redistribute stresses by applying compressive force, leading to refined grain structures and minimizing distortion results in RS.	[24,75,76,171]
Heat treatment (HT)	Grade 91 steel, Ti-6Al-4V	HT post-processing involves controlled heating and cooling cycles to relieve RS. HT is extensively utilized within the aerospace sector to reduce RS in WAAM to produce turbine blades, improving fatigue life and performance.	[82,139,172]
Shot peening	2319 aluminum alloy	Shot peening entails subjecting the surface of a component to bombardment with small, high-velocity particles to induce compressive stresses that counteract tensile RS. It is employed in the automotive sector to enhance the fatigue resistance of WAAM-produced suspension components.	[173,174]
Rolling and laser shock peening	Low carbon steel	The methods eliminate harmful tensile RS at the top of the WAAM wall, thereby enhancing fatigue life and slowing down crack growth rates. The bottom region of the WAAM wall demonstrates improved RS conditions, leading to enhanced fatigue performance, all achieved without surface rolling treatment.	[175]
Rolling	AA2319, S335JR steel	Increased rolling loads result in elevated maximum equivalent plastic strain and deeper penetration of the equivalent plastic strain results in RS.	[32]
Parameter optimization	Al-Cu4.3-Mg1.5 alloy	Adjusting WAAM process parameters, such as deposition speed and layer thickness, can optimize the build conditions to diminish RS. Systematic parameter optimization is applied in the construction industry to reduce RS in large-scale WAAM-printed metal structures.	[36]
Material selection	aluminum alloys	Choosing materials with tailored properties, such as low thermal-expansion coefficients, can minimize RS formation during WAAM. Specialized materials are used in the energy sector to create high-performance WAAM components with reduced RS.	[176,177]
In-process monitoring and control	IN718 Superalloy	Real-time monitoring and control systems adjust process parameters during WAAM to minimize RS formation. In-process monitoring and control are used in aerospace manufacturing to reduce RS variations in critical engine components.	[178]
Hot-rolling and cold-forming	ER70S-6 welding wire	The incorporation of WAAM stiffeners at the flange tips of hot-rolled I-sections is demonstrated to result in the creation of favorable tensile RS, which are beneficial for structural stability, reaching maximum values equivalent to the material's yield strength.	[179]
Peening and UITs	Ti alloy & Al alloy	Through Ultrasonic Impact Treatment (UIT), grain refinement and the randomization of orientation are accomplished, contributing to the enhancement of RS and mechanical strength.	[180]
Rolling	Titanium alloys	Offer substantial advantages such as diminishing RS and distortion, as well as refining grain structure.	[181]

In this study, we explore how various factors such as process parameters, substrate heating, and cooling influence bead appearance formed during WAAM of Inconel 625 on

EN 8 steel. Additionally, the temperature history of the molten pool during deposition using an Infrared (IR) pyrometer can be used to examine how these factors affect the cooling rate, which in turn impacts the bead geometry [137,182]. For the morphological aspect of the beads, it is essential to respect the volume of material supplied and the size of the part [183]. The graphs in Figure 9 illustrate the distribution of published work on approaches used to mitigate residual stress and indicate the frequency of their adoption in WAAM applications. These graphs present different mitigation methods of RS in the WAAM process versus the utilized number of methods published in articles.

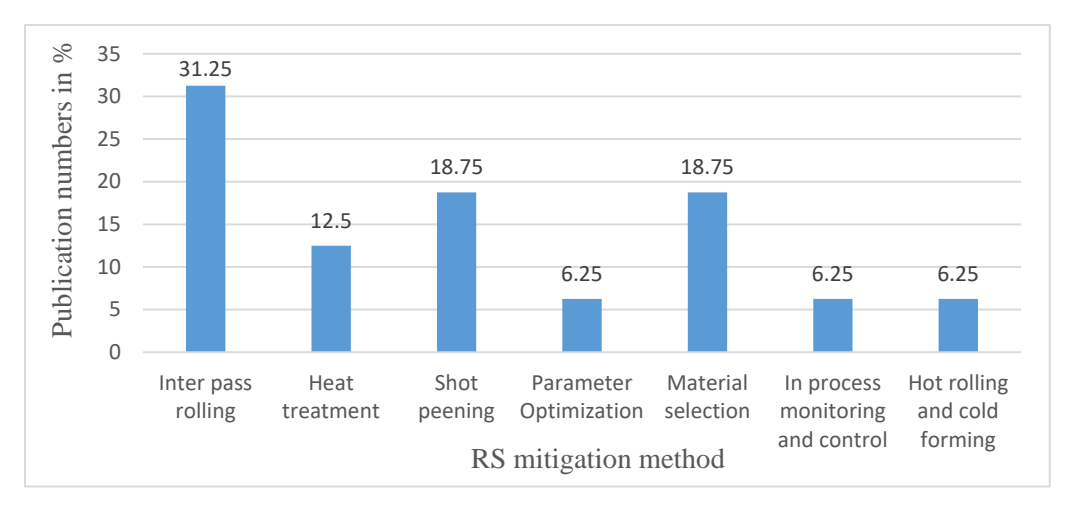


Figure 9. Mitigation method of RS versus publication in percentage.

The graph illustrates the hierarchy of various RS-mitigation techniques on successively deposited layers, while other methods include treatments after production is finished. For instance, inter-pass rolling is mostly applied during the printing process to refine the grain structure, bonding, and adhesion between the consecutive layers of deposit materials. Heat treatment and shot peening are used after fabrication is completed, whereas process monitoring and control are the mitigation methods used during the printing process.

An approach was developed to analyze the shape of the constructed wall, focusing on its inherent symmetry to ensure efficient material utilization. Additionally, it employs thermography techniques to monitor the symmetry of the melting pool [18]. This volume deposition geometry V (m³) can easily be deduced from the path (more specifically the travel length of the welding path l_{scan} (m)), the speed of the wire v_w (m s⁻¹), the diameter of the wire d_w (m), and the welding speed v_t (m s⁻¹) [26,142] as expressed in Equation (4).

$$V = \pi d_w^2 \times v_w \times \frac{l_{scan}}{v_t} \tag{4}$$

To view the particular width (*w*), layer thickness (*h*), and penetration depth (*p*) of the bead from the molten pool during the WAAM process, the shape of the bead is shown in Figure 10. These parameters are important because wider beads offer improved material coverage, leading to a smoother surface finish, while maintaining a controlled bead height minimizes surface irregularities for a smoother finish. Therefore, a modeling of the bead profile is required to establish the relationship among different process parameters. Some studies consider the shapes of beads formed in the WAAM process as ellipses [184,185]. The WAAM process constructs intricate parts by layering weld beads. It is vital to model both individual weld beads and the overlapping of multiple beads to ensure superior surface quality and dimensional precision in the fabricated parts. This begins by developing models for single weld beads using diverse curve-fitting techniques [186,187].

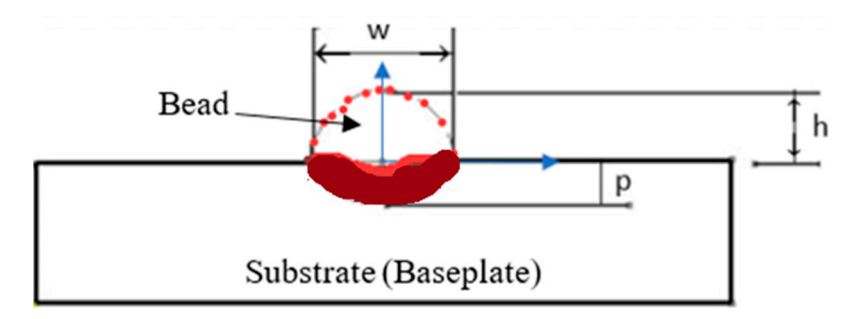


Figure 10. Bead formation of the parabolic profile during the WAAM process.

The geometric representation of different overlapping beads, combined with an algorithm, determines the process conditions required for both materials to achieve consistent bead-layer heights [188]. A geometrically flawed segment of a bead, or geometric defect, is a flaw resulting in voids within the final printed part because of incomplete fusion between two irregularly shaped overlapping bead segments [189]. It is preferable to write the same parabola in terms of the process parameters v_w , wire feed speed, and v_t - torch speed. The geometric configuration of the weld bead created through WAAM differs from that of conventional welding methods [190,191]. The bead profile on the substrate can be considered as a symmetric parabola shape, which is provided in Figure 10 and presented in Equation (5).

$$y = a + cx^2 \tag{5}$$

To solve for a and c in Equation (5), the thickness (height) and width of the beads are substituted into the parabola equation to find the constants a and c. The turning points, or vertex, are at (0, a) for this form of the equation. The parabola is concave downwards because the result of c < 0, as depicted in Figure 10, and the bead profile expressed as a parabolic equation can be solved as Equation (6).

$$a = h; c = -\frac{4h}{w^2}$$

$$y = h \left[1 - \left(\frac{2hx}{w} \right)^2 \right]$$
(6)

The area of a bead (area of the parabolic bead) relative to its geometric parametric is obtained from Equation (7).

$$A = \frac{2hw}{3} \tag{7}$$

The volume flow rate is expressed in Equation (8),

$$Q = \frac{2}{3}hw \times v_t \tag{8}$$

For the wire, when the molten pool flows, the volume flow rate is provided by Equation (9).

$$Q = \frac{\pi}{4} d_w^2 \times v_w \tag{9}$$

where d_w is the wire diameter and v_w is the speed of the wire. Equations (8) and (9), the width-w of the bead is determined from Equation (10).

$$w = \frac{3\pi d_w^2 v_w}{8hv_t} \tag{10}$$

From Equation (10), replacing for w in Equation (6) will provide Equation (11).

$$y = h \left[1 - \left(\frac{16hv_t x}{3\pi v_w d_w^2} \right)^2 \right] \tag{11}$$

For the different wire diameters, the beads formed vary in thickness and width. However, the shape of the deposited bead is greatly influenced by many welding parameters, including torch angle, wire travel speed, filler-feed rate, and cooling conditions [192]. For a particular layer thickness (h), bead width (w), and torch speed (v_t), the volumetric flow rate (Q) required for complete filling is provided by Equation (12).

$$Q = v_t w h (12)$$

Setting the optimum parametric in the WAAM process would be advantageous for the gradual deposition of weld beads layer by layer in the AM of components [193,194]. Koli et al. [128] studied the WAAM products made of wire of SS308L with a 1.2 mm diameter used to manufacture the samples. The parameters, such as welding speed, arc current, and shielding gas-flow rate, were the most influential in affecting the multiple responses of WAAM products.

The practical applications of components printed by WAAM processes are mainly applicable in the automotive [155], aerospace [195], naval, and defense [196,197] industries, which use materials like aluminum due to their high quality and strength with less mass. Generally, WAAM is highly demanded across industries such as automotive, aerospace, chemical plants, maritime, nuclear, shipbuilding, and energy, where it is utilized for fabricating components like aircraft parts, automotive chassis, and marine propellers [8,65,88,148,151,198–204]. The WAAM process in these industries widely used aluminum alloy series such as $2\times\times\times$ (Al-Cu), $4\times\times\times$ (Al-Si), and $5\times\times\times$ (Al-Mg) [199,205,206]. Aerospace components produced in the WAAM process, such as turbine blades, airfoils, and structural elements, need to be carefully controlled in the RS to prevent premature failure and maintain high performance standards [86,129,207,208]. WAAM is also used for producing engine parts like cylinder heads and pistons [129].

6. Discussion

Besides the measurement of RS mentioned earlier, certain welding-related defects may potentially occur in WAAMed components. These measurements include many factors that influence the magnitudes of the RS WAAM, which are described in Table 1 with several references. The inclusions primarily consist of three classifications of RS measuring methods, which are discussed in Section 3.4. Of these three, non-destructive measuring techniques are mostly applicable. However, in large samples, the strain of certain components may be difficult to determine or cannot be precisely identified due to variations of dissimilar RS in the penetration depth-beam light through the components [209]. Still, further research is required to thoroughly examine the RS present in WAAM products, resulting from different process parameters. Post-fabrication heat treatment processes can significantly impact the elimination of defects. Though many defects could be eliminated in WAAMed products, RS was only minimized to the greatest extent possible through heat treatment [137] and other processes mentioned in Table 4.

The quality of metal components fabricated in WAAM relies seriously on key parameters such as travel speed, heat input, wire-feed rate, deposition direction, material properties, etc., and others are mentioned in Table 1. While high heat input is necessary to achieve a rapid deposition rate in WAAM, it also presents challenges like RS and distortions. Therefore, managing heat input becomes crucial, especially when fabricating large metal components using WAAM, as it directly impacts both deposition rate and structural integrity [1,47].

6.1. Challenges and Limitations

Like any manufacturing technique, WAAM comes with its own set of challenges and limitations in the measurement and control of RS. It can be used to fabricate complex geometries, which makes it difficult to predict and measure RS accurately, especially in intricate structures. WAAM products often exhibit heterogeneous microstructures and material properties due to the fast solidification and thermal cycles experienced during deposition. The variations such as material composition, grain structure, and phase transformations can influence the magnitude and distribution of RS, complicating measurement and interpretation. Measuring RS in the products of WAAM poses several challenges due to the unique characteristics of the process of manufacturing and the resulting material properties. For example, non-destructive testing techniques such as ultrasonic testing or X-ray diffraction are promising for measuring RS in WAAM products; adapting these techniques to the unique characteristics of additive manufacturing materials and geometries presents technical challenges. The common challenge during the test is the capacity of beam light-penetration depth dimensions through the printed products. WAAM involves the successive deposition of layers of material, which can result in anisotropic RS distributions. Measuring and characterizing these complex stress patterns accurately requires advanced techniques capable of analyzing stress variations in different directions and depths within the material [210].

The properties and behavior of different materials can vary significantly in different manners and make it challenging to establish a universal approach for RS measurement and control. Management of RS is a critical aspect in the WAAM to ensure the quality and performance of the manufactured components. There were limited industry standards for measuring and controlling RS in the WAAM. The absence of standardized procedures can hinder the adoption of this technology in critical applications. Many investigations cannot provide a specific magnitude of RS. Rather, they indicate numerical results and show the character throughout the fabrication operations of WAAM by modeling.

Quantifying this RS is not assigned for all process and welding parameters. For instance, it is not assigned from the input parameters like wire diameter, art welding directions, length, width, thickness, and volume of the products, there is a comparison of the printed components. Likewise, it is not assigned from parameters related to welding, such as speed of welding, welding gas, gas-flow rate, volts, peak currents, and shielding gas [1,4]. The techniques used in past investigations for measuring RS in the WAAMed products are already listed in Table 2.

In the other case, shielding gas, types of shielding gas, and the shielding gas flow rate affect the distribution and amount of RS in products of WAAM. Similarly, the shielding gas types with their flow rate, such as argon and helium, and reactive gases like carbon dioxide and oxygen can have significant impacts on RS formation in WAAM products [3,138,149]. However, researchers did not identify the optimum amount of the shielding gas and types of shielding gas with other processes and input parameters during the WAAM process. Additionally, several reasons that make RS in WAAM are rapid heating and cooling, multilayer deposition, process parameters, material phase transformations, and part geometry.

The literature review, in general, indicates that continuous investigation and improvement in these areas are essential for advancing the understanding and control of RS within WAAM product applications.

6.2. Future Directions

Challenges and limitations for controlling RS in products of WAAM are discussed in Section 6.1. Based on the measurements, mitigations, and limitations found in the past research, which can be mentioned and recommended, more studies in future investigations could focus on optimizing the parameters of the WAAM process. By elucidating the intricate relationship between process parameters in WAAM and RS, this review contributes and leads to optimizing the process of parameters, using RS measurement techniques and the

assurance of product reliability [69]. Likewise, some of the RS measuring methods, which were not performed in the products of WAAM in past research, are:

(1) Non-destructive methods

(2) Semi-destructive methods

Destructive methods

- Ultrasonic Waves
- Magnetic Barkhausen
- Ring Core
- Deep-Hole Method
- Bridge Curvature
- Sectioning Techniques
- Slitting or Crack Compliance

In another way, the filler wire diameter directly affects the deposition rate and heat generated in WAAM. Larger wire diameters typically result in higher deposition rates but also lead to increased thermal input rate per unit length. This increased heat input can influence the cooling gradients and heat input gradients within the deposited material, affecting the spread and extent of RS. The influence of wire diameter over the molten pool deposition to form beads is described in Section 6 using formulas to present the relationships between height and width throughout the WAAM process. For the significant impact of wire size, the optimum size of wire diameters on the RS in the products of WAAM has not been identified in past investigations. Also, among the categories of measuring RS, the appropriate techniques and limitations with formed-bead geometry are not studied.

Since past research is not inclusive regarding material dependence, methodology modifications, application area, and related research issues of WAAM in the existing literature, there is ample opportunity for upcoming research to explore various possibilities, including:

- 1. Most researchers frequently used non-destructive methods like XRd, ND, and some other semi-destructive and fully destructive techniques of measuring RS in components' WAAM. Thus, future studies can perform those techniques listed above.
- In the future, researchers should determine the most suitable quantity and varieties
 of shielding gas, in addition to other process and input parameters, throughout the
 WAAM processes.
- 3. As explained in Section 5, the mathematical formula provides a particular formation of bead profile and the relationship of wire diameter with the width and thickness (height) of beads. As a result, the wire diameter, thickness, and width of beads can vary. Consequently, heat distribution of the process results in a variation of RS in WAAM parts. Therefore, future research can focus on a variety of wire diameters to reduce RS in WAAM parts with less wire diameter.
- 4. Materials' weld ability depends on their physical properties that influence the accumulation of RS in products of WAAM. In the future, further research endeavors should aim to investigate these physical properties of materials, which are listed in Table 3, and other robot-adjustable effects to RS-fabricated components through WAAM.

7. Conclusions

In conclusion, this literature review has delved deeply into the extensive research surrounding the investigation and measurement of RS in WAAM products, with a specific emphasis on the influence of fabrication parameters. The significance of RS in determining the material characteristics and structural integrity of WAAM components has been underscored throughout the review work. Moreover, the study has provided an all-inclusive summary of key findings, measurement methods, problems, and future directions in the WAAM dynamic field.

The review highlights the critical role of RS in shaping the dimensional constancy of WAAM products, emphasizing the necessity of precise measurement and control for effective utilization. Synthesizing diverse research studies, techniques, and methodologies, the review work has offered a valuable understanding of the present research status in this domain. Furthermore, this review serves as a guide for future researchers to use the other RS measurement techniques, those that have not been performed yet, and compare previous techniques used in the literature. In particular, the review indicated that no significant

work has been reported on the impact of RS in WAAM-fabricated parts on fatigue and creep strengths, which we would like to address in our continuing works in this area. To measure RS WAAMed products, experimental methods, including semi-destructive (only hole drilling), destructive (contour method), and non-destructive techniques (such as neutron crystallography and X-ray diffraction, digital image correlation, and synchrotron X-ray diffraction) have been reported.

Overall, this review is inclusive of examining and measuring RS techniques in WAAM products based on input parameters and other influences of RS products. Through meticulous evaluation and coordination of the existing literature, this review underscores the importance of understanding the factors influencing and mitigating methods of RS in products of WAAM.

Author Contributions: The roles of the authors in this study are outlined as follows: F.D.G. came up with the title and contributed to conceptualization, methodology, investigation, and original draft preparation. H.G.L. contributed to the conceptualization and provided resources, supervision, project administration, editing, a review of the manuscript, and a securing of funding. Y.W.A. participated in editing and reviewing the manuscript. M.D.H. has also participated in organizing and data analysis in the manuscript. All authors have read and agreed to the published version of the manuscript.

Funding: This study received backing from the INDMET initiative under grant number 62862, which was financed through the NORHED II program.

Data Availability Statement: The original contributions presented in the study are included in the article, further inquiries can be directed to the corresponding authors.

Conflicts of Interest: The authors declare no conflict of interest.

References

- 1. Kumar, M.B.; Sathiya, P.; Senthil, S.M. A critical review of wire arc additive manufacturing of nickel-based alloys: Principles, process parameters, microstructure, mechanical properties, heat treatment effects, and defects. *J. Braz. Soc. Mech. Sci. Eng.* **2023**, 45, 1–27.
- 2. Tangestani, R.; Farrahi, G.H.; Shishegar, M.; Aghchehkandi, B.P.; Ganguly, S.; Mehmanparast, A. Effects of Vertical and Pinch Rolling on Residual Stress Distributions in Wire and Arc Additively Manufactured Components. *J. Mater. Eng. Perform.* **2020**, 29, 2073–2084. [CrossRef]
- 3. Derekar, K.S. Aspects of Wire Arc Additive Manufacturing (WAAM) of Alumnium Alloy 5183. Ph.D. Thesis, Coventry University, Coventry, UK, 2020; pp. 1–227.
- 4. Rodrigues, T.A.; Duarte, V.; Miranda, R.M.; Santos, T.G.; Oliveira, J.P. Current Status and Perspectives on Wire and Arc Additive Manufacturing (WAAM). *Materials* **2019**, 12, 1121. [CrossRef]
- 5. Laghi, V.; Palermo, M.; Gasparini, G.; Veljkovic, M.; Trombetti, T. Assessment of design mechanical parameters and partial safety factors for Wire-and-Arc Additive Manufactured stainless steel. *Eng. Struct.* **2020**, 225, 111314. [CrossRef]
- 6. Cunningham, C.R.; Flynn, J.M.; Shokrani, A.; Dhokia, V.; Newman, S.T. Invited review article: Strategies and processes for high quality wire arc additive manufacturing. *Addit. Manuf.* **2018**, 22, 672–686. [CrossRef]
- 7. Klobčar, D.; Baloš, S.; Bašić, M.; Djurić, A.; Lindič, M.; Ščetinec, A. WAAM and Other Unconventional Metal Additive Manufacturing Technologies. *Adv. Technol. Mater.* **2020**, *45*, 1–9. [CrossRef]
- 8. Mathews, R.; Karandikar, J.; Tyler, C.; Smith, S. Residual stress accumulation in large-scale Ti-6Al-4V wire-arc additive manufacturing. *Procedia CIRP* **2024**, *121*, 180–185. [CrossRef]
- 9. Wu, B.; Pan, Z.; van Duin, S.; Li, H. Thermal Behavior in Wire Arc Additive Manufacturing: Characteristics, Effects and Control. In *Transactions on Intelligent Welding Manufacturing*; Springer: Singapore, 2019; pp. 3–18.
- 10. Williams, S.W.; Martina, F.; Addison, A.C.; Ding, J.; Pardal, G.; Colegrove, P. Wire + Arc additive manufacturing. *Mater. Sci. Technol.* **2016**, 32, 641–647. [CrossRef]
- 11. Jimenez, X.; Dong, W.; Paul, S.; Klecka, M.A.; To, A.C. Residual Stress Modeling with Phase Transformation for Wire Arc Additive Manufacturing of B91 Steel. *JOM* **2020**, 72, 4178–4186. [CrossRef]
- 12. Jin, W.; Zhang, C.; Jin, S.; Tian, Y.; Wellmann, D.; Liu, W. Wire Arc Additive Manufacturing of Stainless Steels: A Review. *Appl. Sci.* 2020, *10*, 1563. [CrossRef]
- 13. Huang, W.; Wang, Q.; Ma, N.; Kitano, H. Distribution characteristics of residual stresses in typical wall and pipe components built by wire arc additive manufacturing. *J. Manuf. Process.* **2022**, *82*, 434–447. [CrossRef]
- Mohan Kumar, S.; Rajesh Kannan, A.; Pravin Kumar, N.; Pramod, R.; Siva Shanmugam, N.; Vishnu, A.S.; Channabasavanna, S.G. Microstructural Features and Mechanical Integrity of Wire Arc Additive Manufactured SS321/Inconel 625 Functionally Gradient Material. J. Mater. Eng. Perform. 2021, 30, 5692–5703. [CrossRef]

15. Kumar, V.; Singh, A.; Bishwakarma, H.; Mandal, A. Simulation of Metallic Wire-Arc Additive Manufacturing (Waam) Process Using Simufact Welding Software. *J. Manuf. Eng.* **2023**, *18*, 080–085. [CrossRef]

- 16. Knezović, N.; Topić, A. Wire and Arc Additive Manufacturing (WAAM)—A New Advance in Manufacturing. In *Lecture Notes in Networks and Systems*; Springer International Publishing: New York, NY, USA, 2019; Volume 42, pp. 65–71.
- 17. Costello, S.C.A.; Cunningham, C.R.; Xu, F.; Shokrani, A.; Dhokia, V.; Newman, S.T. The state-of-the-art of wire arc directed energy deposition (WA-DED) as an additive manufacturing process for large metallic component manufacture. *Int. J. Comput. Integr. Manuf.* 2023, 36, 469–510. [CrossRef]
- 18. Barath Kumar, M.D.; Manikandan, M. Assessment of Process, Parameters, Residual Stress Mitigation, Post Treatments and Finite Element Analysis Simulations of Wire Arc Additive Manufacturing Technique. Metals and Materials International. *Korean Inst. Met. Mater.* 2022, 28, 54–111. [CrossRef]
- 19. Paskual, A.; Alvarez, P.; Suárez, A. Study on Arc Welding Processes for High Deposition Rate Additive Manufacturing. *Procedia CIRP* **2018**, *68*, 358–362.
- 20. Shukla, P.; Dash, B.; Kiran, D.V.; Bukkapatnam, S. Arc Behavior in Wire Arc Additive Manufacturing Process. *Procedia Manuf.* **2020**, *48*, 725–729. [CrossRef]
- 21. Zhao, X.F.; Wimmer, A.; Zaeh, M.F. Experimental and simulative investigation of welding sequences on thermally induced distortions in wire arc additive manufacturing. *Rapid Prototype J.* **2023**, 29, 53–63. [CrossRef]
- 22. Cambon, C.; Bendaoud, I.; Rouquette, S.; Soulié, F. A WAAM benchmark: From process parameters to thermal effects on weld pool shape, microstructure and residual stresses. *Mater. Today Commun.* **2022**, *33*, 104235. [CrossRef]
- 23. Hönnige, J.; Seow, C.E.; Ganguly, S.; Xu, X.; Cabeza, S.; Coules, H.; Williams, S. Study of residual stress and microstructural evolution in as-deposited and inter-pass rolled wire plus arc additively manufactured Inconel 718 alloy after ageing treatment. *Mater. Sci. Eng. A* **2020**, *801*, 140368. [CrossRef]
- 24. Hönnige, J.R.; Colegrove, P.A.; Ganguly, S.; Eimer, E.; Kabra, S.; Williams, S. Control of Residual Stress and Distortion in Aluminium Wire + Arc Additive Manufacture with Rolling. *Addit Manuf.* **2018**, 22, 775–783. [CrossRef]
- 25. Schroepfer, K.W.D.; Wildenhain, R.S.; Kannengiesser, A.H.T.; Hensel, A.K.J. Influence of the WAAM process and design aspects on residual stresses in high—Strength structural steels. *Weld World* **2023**, *67*, 987–996.
- Geng, R.; Du, J.; Wei, Z.; Xu, S.; Ma, N. Modelling and experimental observation of the deposition geometry and microstructure evolution of aluminum alloy fabricated by wire-arc additive manufacturing. J. Manuf. Process. 2021, 64, 369–378. [CrossRef]
- 27. Klein, T.; Spoerk-Erdely, P.; Schneider-Broeskamp, C.; Oliveira, J.P.; Faria, G.A. Residual Stresses in a Wire and Arc-Directed Energy-Deposited Al–6Cu–Mn (ER2319) Alloy Determined by Energy-Dispersive High-Energy X-ray Diffraction. *Met. Mater. Trans. A* 2024, 55, 736–744. [CrossRef]
- 28. Ermakova, A.; Mehmanparast, A.; Ganguly, S.; Razavi, N.; Berto, F. Investigation of mechanical and fracture properties of wire and arc additively manufactured low carbon steel components. *Theor. Appl. Fract. Mech.* **2020**, *109*, 102685. [CrossRef]
- 29. Derekar, K.S. A review of wire arc additive manufacturing and advances in wire arc additive manufacturing of aluminium. *Mater. Sci. Technol.* **2018**, 34, 895–916. [CrossRef]
- 30. Taşdemir, A.; Nohut, S. An overview of wire arc additive manufacturing (WAAM) in shipbuilding industry. *Ships Offshore Struct*. **2020**, *16*, 1–18. [CrossRef]
- 31. Müller, J.; Grabowski, M.; Müller, C.; Hensel, J.; Unglaub, J.; Thiele, K.; Kloft, H.; Dilger, K. Design and Parameter Identification of Wire and Arc Additively Manufactured (WAAM) Steel Bars for Use in Construction. *Metals* **2019**, *9*, 725. [CrossRef]
- 32. Abbaszadeh, M.; Hönnige, J.R.; Martina, F.; Neto, L.; Kashaev, N.; Colegrove, P.; Williams, S.; Klusemann, B. Numerical Investigation of the Effect of Rolling on the Localized Stress and Strain Induction for Wire + Arc Additive Manufactured Structures. J. Mater. Eng. Perform. 2019, 28, 4931–4942. [CrossRef]
- 33. Song, S.S.; Chen, J.; Quan, G.; Ye, J.; Zhao, Y. Numerical analysis and design of concrete-filled wire arc additively manufactured steel tube under axial compression. *Eng. Struct.* **2024**, *301*, 117294. [CrossRef]
- 34. Wu, Q.; Mukherjee, T.; De, A.; DebRoy, T. Residual stresses in wire-arc additive manufacturing—Hierarchy of influential variables. *Addit. Manuf.* **2020**, *35*, 101355. [CrossRef]
- 35. Ding, D.; Pan, Z.; Cuiuri, D.; Li, H. Wire-feed additive manufacturing of metal components: Technologies, developments and future interests. *Int. J. Adv. Manuf. Technol.* **2015**, *81*, 465–481. [CrossRef]
- 36. Jafari, D.; Vaneker, T.H.J.; Gibson, I. Wire and arc additive manufacturing: Opportunities and challenges to control the quality and accuracy of manufactured parts. *Mater. Des.* **2021**, 202, 109471. [CrossRef]
- 37. Wu, B.; Pan, Z.; Chen, G.; Ding, D.; Yuan, L.; Cuiuri, D.; Li, H. Mitigation of thermal distortion in wire arc additively manufactured Ti6Al4V part using active interpass cooling. *Sci. Technol. Weld. Join.* **2019**, 24, 484–494. [CrossRef]
- 38. Rozaimi, M.; Yusof, F. Research challenges, quality control and monitoring strategy for Wire Arc Additive Manufacturing. *J. Mater. Res. Technol.* **2023**, 24, 2769–2794.
- 39. Ahmad, B.; Zhang, X.; Guo, H.; Fitzpatrick, M.E.; Neto, L.M.S.C.; Williams, S. Influence of Deposition Strategies on Residual Stress in Wire + Arc Additive Manufactured Titanium Ti-6Al-4V. *Metals* **2022**, *12*, 253. [CrossRef]
- 40. Schönegger, S.; Moschinger, M.; Enzinger, N. Computational welding simulation of a plasma wire arc additive manufacturing process for high-strength steel. *Eur. J. Mater.* **2024**, *4*, 2297051. [CrossRef]
- 41. Qvale, P.; Njaastad, E.B.; Bræin, T.; Ren, X. A fast simulation method for thermal management in wire arc additive manufacturing repair of a thin-walled structure. *Int. J. Adv. Manuf. Technol.* **2024**, *132*, 1573–1583. [CrossRef]

42. Wang, C.; Suder, W.; Ding, J.; Williams, S. The effect of wire size on high deposition rate wire and plasma arc additive manufacture of Ti-6Al-4V. *J. Am. Acad. Dermatol.* **2021**, 288, 116842. [CrossRef]

- 43. Gupta, A.K.; Bansal, H.; Madan, A. Study on CNC Wire Arc Additive Manufacturing process for Higher Deposition Rate and Mechanical Strength. *Adv. Robot. Autom.* **2022**, *10*, 9695.
- 44. Ananda, P.A. WAAM Application for EPC Company. MATEC Web Conf. 2019, 269, 05002. [CrossRef]
- 45. Li, Y.; Dong, Z.; Miao, J.; Liu, H.; Babkin, A.; Chang, Y. Forming accuracy improvement in wire arc additive manufacturing (WAAM): A review. *Rapid Prototyp. J.* **2022**, *29*, 673–686. [CrossRef]
- 46. Chaurasia, M.; Sinha, M.K. *Investigations on Process Parameters of Wire Arc Additive Manufacturing (WAAM): A Review;* Lecture Notes in Mechanical Engineering; Springer Nature: Singapore, 2021; pp. 845–853.
- 47. Gowthaman, P.S.; Jeyakumar, S.; Sarathchandra, D. Effect of Heat Input on Microstructure and Mechanical Properties of 316L Stainless Steel Fabricated by Wire Arc Additive Manufacturing. *J. Mater. Eng. Perform.* **2024**, *33*, 5536–5546. [CrossRef]
- 48. Tomar, B.; Shiva, S.; Nath, T. A review on wire arc additive manufacturing: Processing parameters, defects, quality improvement and recent advances. *Mater. Today Commun.* **2022**, *31*, 103739. [CrossRef]
- 49. Voropaev, A.; Korsmik, R.; Tsibulskiy, I. Features of Filler Wire Melting and Transferring in Wire-Arc Additive Manufacturing of Metal Workpieces. *Materials* **2021**, *14*, 5077. [CrossRef] [PubMed]
- 50. Chen, C.; He, H.; Zhou, S.; Lian, G.; Huang, X.; Feng, M. Prediction of multi-bead profile of robotic wire and arc additive manufactured components recursively using axisymmetric drop shape analysis. *Virtual Phys. Prototyp.* **2023**, *18*, 1–24. [CrossRef]
- 51. Ayed, A.; Valencia, A.; Bras, G.; Bernard, H.; Michaud, P.; Balcaen, Y.; Alexis, J. Effects of WAAM Process Parameters on Metallurgical and Mechanical Properties of Ti-6Al-4V Deposits. In *Advances in Materials, Mechanics and Manufacturing: Proceedings of the Second International Conference on Advanced Materials, Mechanics and Manufacturing (A3M'2018), Hammamet, Tunisia, 17–19 December 2018*; Lecture Notes in Mechanical Engineering; Springer International Publishing: Berlin/Heidelberg, Germany, 2020; pp. 26–35.
- 52. Mai, D.S.; Doan, T.K.; Paris, H. Engineering Science and Technology, an International Journal Wire and arc additive manufacturing of 308L stainless steel components: Optimization of processing parameters and material properties. *Eng. Sci. Technol. Int. J.* **2021**, 24, 1015–1026.
- 53. Lin, Z.; Goulas, C.; Ya, W.; Hermans, M.J. Microstructure and Mechanical Properties of Medium Carbon Steel Deposits Obtained via Wire and Arc Additive Manufacturing Using Metal-Cored Wire. *Metals* **2019**, *9*, 673. [CrossRef]
- 54. Song, G.H.; Lee, C.M.; Kim, D.H. Investigation of Path Planning to Reduce Height Errors of Intersection Parts in Wire-Arc Additive Manufacturing. *Materials* **2021**, *14*, 6477. [CrossRef]
- 55. Zhou, Z.; Shen, H.; Liu, B.; Du, W.; Jin, J.; Lin, J. Residual thermal stress prediction for continuous tool-paths in wire-arc additive manufacturing: A three-level data-driven method. *Virtual Phys. Prototyp.* **2022**, *17*, 105–124. [CrossRef]
- 56. Guo, C.; Li, G.; Li, S.; Hu, X.; Lu, H.; Li, X.; Xu, Z.; Chen, Y.; Li, Q.; Lu, J.; et al. Additive manufacturing of Ni-based superalloys: Residual stress, mechanisms of crack formation and strategies for crack inhibition. *Nano Mater. Sci.* **2023**, *5*, 53–77. [CrossRef]
- 57. Scotti, F.M.; Teixeira, F.R.; da Silva, L.J.; de Araújo, D.B.; Reis, R.P.; Scotti, A. Thermal management in WAAM through the CMT Advanced process and an active cooling technique. *J. Manuf. Process.* **2020**, *57*, 23–35. [CrossRef]
- 58. Ahsan, M.R.U.; Tanvir, A.N.M.; Ross, T.; Elsawy, A.; Oh, M.S.; Kim, D.B. Fabrication of bimetallic additively manufactured structure (BAMS) of low carbon steel and 316L austenitic stainless steel with wire + arc additive manufacturing. *Rapid Prototype J.* **2020**, *26*, 519–530. [CrossRef]
- 59. Wu, Q.; Ma, Z.; Chen, G.; Liu, C.; Ma, D.; Ma, S. Obtaining fine microstructure and unsupported overhangs by low heat input pulse arc additive manufacturing. *J. Manuf. Process.* **2017**, 27, 198–206. [CrossRef]
- 60. Doumenc, G.; Couturier, L.; Courant, B.; Paillard, P.; Benoit, A.; Gautron, E.; Girault, B.; Pirling, T.; Cabeza, S.; Gloaguen, D. Investigation of microstructure, hardness and residual stresses of wire and arc additive manufactured 6061 aluminium alloy to cite this version: HAL Id: Hal-03827007. *Materialia* 2022, 25, 101520. [CrossRef]
- 61. Tröger, J.-A.; Hartmann, S.; Treutler, K.; Potschka, A.; Wesling, V. Simulation-based process parameter optimization for wire arc additive manufacturing. *Prog. Addit. Manuf.* **2024**. [CrossRef]
- 62. Nagallapati, V.; Khare, V.K.; Sharma, A.; Simhambhatla, S. Active and Passive Thermal Management in Wire Arc Additive Manufacturing. *Metals* **2023**, *13*, 682. [CrossRef]
- 63. Ahsan, M.; Seo, G.-J.; Fan, X.; Liaw, P.K.; Motaman, S.; Haase, C.; Kim, D.B. Effects of process parameters on bead shape, microstructure, and mechanical properties in wire + arc additive manufacturing of Al0.1CoCrFeNi high-entropy alloy. *J. Manuf. Process.* 2021, 68, 1314–1327. [CrossRef]
- 64. He, T.; Yu, S.; Shi, Y.; Huang, A. Forming and mechanical properties of wire arc additive manufacture for marine propeller bracket. *J. Manuf. Process.* **2020**, 52, 96–105. [CrossRef]
- 65. Su, C.; Chen, X.; Gao, C.; Wang, Y. Effect of heat input on microstructure and mechanical properties of Al-Mg alloys fabricated by WAAM. *Appl. Surf. Sci.* **2019**, *486*, 431–440. [CrossRef]
- 66. Scharf-Wildenhain, R.; Haelsig, A.; Hensel, J.; Wandtke, K.; Schroepfer, D.; Kromm, A.; Kannengiesser, T. Influence of Heat Control on Properties and Residual Stresses of Additive-Welded High-Strength Steel Components. *Metals* 2022, 12, 951. [CrossRef]
- 67. Javadi, Y.; Smith, M.; Venkata, K.A.; Naveed, N.; Forsey, A.; Francis, J.; Ainsworth, R.; Truman, C.; Smith, D.; Hosseinzadeh, F.; et al. Residual stress measurement round robin on an electron beam welded joint between austenitic stainless steel 316L(N) and ferritic steel P91. *Int. J. Press. Vessel. Pip.* **2017**, *154*, 41–57.

68. Saleh, B.; Fathi, R.; Tian, Y.; Radhika, N.; Jiang, J.; Ma, A. Fundamentals and advances of wire arc additive manufacturing: Materials, process parameters, potential applications, and future trends. In *Archives of Civil and Mechanical Engineering*; Springer: London, UK, 2023; Volume 23, pp. 1–71.

- 69. Rosli, N.A.; Alkahari, M.R.; bin Abdollah, M.F.; Maidin, S.; Ramli, F.R.; Herawan, S.G. Review on effect of heat input for wire arc additive manufacturing process. *J. Mater. Res. Technol.* **2021**, *11*, 2127–2145. [CrossRef]
- 70. Li, J.Z.; Alkahari, M.R.; Rosli, N.A.B.; Hasan, R.; Sudin, M.N.; Ramli, F.R. Review of Wire Arc Additive Manufacturing for 3D Metal Printing Review of Wire Arc Additive Manufacturing for 3D Metal Printing. *Int. J. Autom. Technol.* **2019**, *13*, 346–353.
- Woo, W.; Kim, D.-K.; Kingston, E.; Luzin, V.; Salvemini, F.; Hill, M.R. Effect of interlayers and scanning strategies on throughthickness residual stress distributions in additive manufactured ferritic-austenitic steel structure. *Mater. Sci. Eng. A* 2019, 744, 618–629.
- 72. Geng, H.; Li, J.; Gao, J.; Lin, X. Theoretical Model of Residual Stress and Warpage for Wire and Arc Additive Manufacturing Stiffened Panels. *Metals* **2020**, *10*, 666. [CrossRef]
- 73. Rouquette, S.; Cambon, C.; Bendaoud, I.; Soulié, F. Residual stresses in ss316l specimens after deposition of melted filler wire. In Proceedings of the ICRS 11—The 11th International Conference on Residual Stresses, Nancy, France, 27–30 March 2022.
- 74. Kumaran, M.; Senthilkumar, V.; Panicke, C.J.; Shishir, R. Investigating the residual stress in additive manufacturing of repair work by directed energy deposition process on SS316L hot rolled steel substrate. *Mater. Today Proc.* **2021**, 47, 4475–4478. [CrossRef]
- 75. Mishurova, T.; Sydow, B.; Thiede, T.; Sizova, I.; Ulbricht, A.; Bambach, M.; Bruno, G. Residual Stress and Microstructure of a Ti-6Al-4V Wire Arc Additive Manufacturing Hybrid Demonstrator. *Metals* **2020**, *10*, 701. [CrossRef]
- 76. Martina, F.; Roy, M.J.; Szost, B.A.; Terzi, S.; Colegrove, P.A.; Williams, S.W.; Withers, P.J.; Meyer, J.; Hofmann, M. Residual stress of as-deposited and rolled wire + arc additive manufacturing Ti–6Al–4V components. *Mater. Sci. Technol.* **2016**, *32*, 1439–1448. [CrossRef]
- 77. Liu, C.; Lin, C.; Wang, J.; Wang, J.; Yan, L.; Luo, Y.; Yang, M. Residual stress distributions in thick specimens excavated from a large circular wire plus arc additive manufacturing mockup. *J. Manuf. Process.* **2020**, *56*, 474–481.
- 78. Yang, Y.; Jin, X.; Liu, C.; Xiao, M.; Lu, J.; Fan, H.; Ma, S. Residual Stress, Mechanical Properties, and Grain Morphology of Ti-6Al-4V Alloy Produced by Ultrasonic Impact Treatment Assisted Wire and Arc Additive Manufacturing. *Metals* **2018**, *8*, 934. [CrossRef]
- 79. Boruah, D.; Dewagtere, N.; Ahmad, B.; Nunes, R.; Tacq, J.; Zhang, X.; Guo, H.; Verlinde, W.; De Waele, W. Digital Image Correlation for Measuring Full-Field Residual Stresses in Wire and Arc Additive Manufactured Components. *Materials* **2023**, 16, 1702. [CrossRef] [PubMed]
- 80. Rani, K.U.; Kumar, R.; Mahapatra, M.M.; Mulik, R.S.; Świerczyńska, A.; Fydrych, D.; Pandey, C. Wire Arc Additive Manufactured Mild Steel and Austenitic Properties and Residual Stresses. *Materials* **2022**, *15*, 7094. [CrossRef] [PubMed]
- 81. Gao, L.; Chuang, A.C.; Kenesei, P.; Ren, Z.; Balderson, L.; Sun, T. An operando synchrotron study on the effect of wire melting state on solidification microstructures of Inconel 718 in wire-laser directed energy deposition. *Int. J. Mach. Tools Manuf.* **2024**, 194, 104089. [CrossRef]
- 82. Robin, I.K.; Sprouster, D.J.; Sridharan, N.; Snead, L.L.; Zinkle, S.J. Synchrotron based investigation of anisotropy and microstructure of wire arc additive manufactured Grade 91 steel. *J. Mater. Res. Technol.* **2024**, *29*, 5010–5021. [CrossRef]
- 83. Kumar, V.; Mandal, A.; Das, A.K.; Kumar, S. Parametric study and characterization of wire arc additive manufactured steel structures. *Int. J. Adv. Manuf. Technol.* **2021**, *115*, 1723–1733. [CrossRef]
- 84. Shen, C.; Reid, M.; Liss, K.-D.; Pan, Z.; Ma, Y.; Cuiuri, D.; van Duin, S.; Li, H. Neutron diffraction residual stress determinations in Fe3Al based iron aluminide components fabricated using wire-arc additive manufacturing (WAAM). *Addit. Manuf.* 2019, 29, 100774. [CrossRef]
- 85. Rouquette, S.; Cambon, C.; Bendaoud, I.; Cabeza, S.; Soulié, F. Effect of Layer Addition on Residual Stresses of Wire Arc Additive Manufactured Stainless Steel Specimens. *J. Manuf. Sci. Eng.* **2024**, *146*, 1–12. [CrossRef]
- 86. Rodrigues, T.A.; Farias, F.W.C.; Zhang, K.; Shamsolhodaei, A.; Shen, J.; Zhou, N.; Schell, N.; Capek, J.; Polatidis, E.; Santos, T.G.; et al. Wire and arc additive manufacturing of 316L stainless steel/Inconel 625 functionally graded material: Development and characterization. *J. Mater. Res. Technol.* 2022, 21, 237–251. [CrossRef]
- 87. Théodore, J.; Couturier, L.; Girault, B.; Cabeza, S.; Pirling, T.; Frapier, R.; Bazin, G.; Courant, B. Relationship between microstructure, and residual strain and stress in stainless steels in-situ alloyed by double-wire arc additive manufacturing (D-WAAM) process. *Materialia* 2023, 30, 101850. [CrossRef]
- 88. Kumar, M.B.; Manikandan, M. Evaluation of Microstructure, Residual Stress, and Mechanical Properties in Different Planes of Wire + Arc Additive Manufactured Nickel—Based Superalloy. *Met. Mater. Int.* **2022**, *28*, 3033–3056. [CrossRef]
- 89. Welding Consumables for Steels with Yield Strength > 460 MPa. Available online: https://www.welmet.cz/wp-content/uploads/2019/04/2-SM-pro-oceli-s-mez%C3%AD-kluzu-nad-460-MPa.pdf (accessed on 26 June 2024).
- 90. Sun, J.; Hensel, J.; Köhler, M.; Dilger, K. Residual stress in wire and arc additively manufactured aluminum components. *J. Manuf. Process.* **2021**, *65*, 97–111. [CrossRef]
- 91. Rodrigues, T.A.; Farias, F.W.C.; Avila, J.A.; Maawad, E.; Schell, N.; Santos, T.G.; Oliveira, J.P. Effect of heat treatments on Inconel 625 fabricated by wire and arc additive manufacturing: An in situ synchrotron X-ray diffraction analysis. *Sci. Technol. Weld. Join.* 2023, 28, 534–539. [CrossRef]

92. Wandtke, K.; Becker, A.; Schroepfer, D.; Kromm, A.; Kannengiesser, T.; Scharf-Wildenhain, R.; Haelsig, A.; Hensel, J. Residual Stress Evolution during Slot Milling for Repair Welding and Wire Arc Additive Manufacturing of High-Strength Steel Components. *Metals* 2024, 14, 82. [CrossRef]

- 93. Wu, Q.; Mukherjee, T.; Liu, C.; Lu, J.; DebRoy, T. Residual stresses and distortion in the patterned printing of titanium and nickel alloys. *Addit. Manuf.* **2019**, *29*, 100808. [CrossRef]
- 94. Han, Y. A Finite Element Study of Wire Arc Additive Manufacturing of Aluminum Alloy. Appl. Sci. 2024, 14, 810. [CrossRef]
- 95. Khaled, H.; Abusalma, J. Parametric Study of Residual Stresses in Wire and Arc Additive Manufactured Parts. Master's Thesis, Old Dominion University, Norfolk, VA, USA, 2020.
- 96. Saadatmand, M.; Talemi, R. Study on the thermal cycle of Wire Arc Additive Manufactured (WAAM) carbon steel wall using numerical simulation. *Frat. Ed Integrita Strutt.* **2020**, *14*, 98–104. [CrossRef]
- 97. Eisazadeh, H.; Achuthan, A.; Goldak, J.; Aidun, D. Effect of material properties and mechanical tensioning load on residual stress formation in GTA 304-A36 dissimilar weld. *J. Mater. Process. Technol.* **2015**, 222, 344–355. [CrossRef]
- 98. Nezamdost, M.R.; Esfahani, M.R.N.; Hashemi, S.H.; Mirbozorgi, S.A. Investigation of temperature and residual stresses field of submerged arc welding by finite element method and experiments. *Int. J. Adv. Manuf. Technol.* **2016**, *87*, 615–624. [CrossRef]
- 99. Huang, H.; Ma, N.; Chen, J.; Feng, Z.; Murakawa, H. Toward large-scale simulation of residual stress and distortion in wire and arc additive manufacturing. *Addit. Manuf.* **2020**, *34*, 101248. [CrossRef]
- 100. Han, Y.S. Wire Arc Additive Manufacturing: A Study of Process Parameters Using Multiphysics Simulations. *Materials* **2023**, 16, 7267. [CrossRef] [PubMed]
- 101. Jia, J.; Zhao, Y.; Dong, M.; Wu, A.; Li, Q. Numerical simulation on residual stress and deformation for WAAM parts of aluminum alloy based on temperature function method. *Trans. China Weld. Inst.* **2020**, *29*, 1–8.
- 102. Feng, G.; Wang, H.W.Y.; Deng, D.; Zhang, J. Numerical Simulation of Residual Stress and Deformation in Wire Arc Additive Manufacturing. *Crystals* **2022**, *12*, 803. [CrossRef]
- 103. Graf, M.; Pradjadhiana, K.P.; Hälsig, A.; Manurung, Y.H.P.; Awiszus, B. Numerical simulation of metallic wire arc additive manufacturing (WAAM). In *AIP Conference Proceedings*; AIP Publishing: Long Island, NY, USA, 2018; Volume 960, p. 140010.
- 104. Ahmad, S.N.; Manurung, Y.H.; Mat, M.F.; Minggu, Z.; Jaffar, A.; Pruller, S.; Leitner, M. FEM simulation procedure for distortion and residual stress analysis of wire arc additive manufacturing. In *IOP Conference Series: Materials Science and Engineering*; IOP Publishing: Bristol, UK, 2020; Volume 834, p. 012083.
- 105. Cadiou, S.; Courtois, M.; Carin, M.; Berckmans, W.; Le masson, P. 3D heat transfer, fluid flow and electromagnetic model for cold metal transfer wire arc additive manufacturing (Cmt-Waam). *Addit. Manuf.* **2020**, *36*, 101541. [CrossRef]
- 106. Drexler, H.; Haunreiter, F.; Raberger, L.; Reiter, L.; Hütter, A.; Enzinger, N. Numerical Modeling of Distortions and Residual Stresses During Wire Arc Additive Manufacturing of an ER 5183 Alloy with Weaving Deposition. *BHM Bergund Hüttenmännische Monatshefte* 2024, 169, 38–47. [CrossRef]
- 107. Bonifaz, E.A.; Palomeque, J.S. A mechanical model in wire + Arc additive manufacturing process. *Prog. Addit. Manuf.* **2020**, *5*, 163–169. [CrossRef]
- 108. Reyes-Gordillo, E.; Gómez-Ortega, A.; Morales-Estrella, R.; Pérez-Barrera, J.; Gonzalez-Carmona, J.; Escudero-García, R.; Alvarado-Orozco, J. Effect of Cold Metal Transfer Parameters during Wire Arc Additive Manufacturing of Ti6Al4V Multi-Layer Walls. 2022. Available online: https://www.researchsquare.com/article/rs-1946459/v1 (accessed on 26 June 2024).
- 109. Silva, W.F. Evaluation of the properties of Inconel [®] 625 preforms manufactured using WAAM technology. *Res. Sq.* **2024**. Available online: https://www.researchsquare.com/article/rs-3591195/v1 (accessed on 26 June 2024).
- 110. Derekar, K.S.; Addison, A.; Joshi, S.S.; Zhang, X.; Lawrence, J.; Xu, L.; Melton, G.; Griffiths, D. Effect of pulsed metal inert gas (pulsed-MIG) and cold metal transfer (CMT) techniques on hydrogen dissolution in wire arc additive manufacturing (WAAM) of aluminium. *Int. J. Adv. Manuf. Technol.* 2020, 107, 311–331. [CrossRef]
- 111. Rosli, N.A.; Alkahari, M.R.; Ramli, F.R.; Sudin, M.N.; Maidin, S. Influence of Process Parameters in Wire and Arc Additive Manufacturing (WAAM). *Process. J. Mech. Eng.* **2020**, *17*, 69–78. [CrossRef]
- 112. Derekar, K.S.; Ahmad, B.; Zhang, X.; Joshi, S.S.; Lawrence, J.; Xu, L.; Melton, G.; Addison, A. Effects of Process Variants on Residual Stresses in Wire Arc Additive Manufacturing of Aluminum Alloy 5183. *J. Manuf. Sci. Eng. Trans.* 2022, 144, 071005. [CrossRef]
- 113. Yuan, Q.; Liu, C.; Wang, W.; Wang, M. Residual stress distribution in a large specimen fabricated by wire-arc additive manufacturing. Sci. Technol. Weld. Join. 2023, 28, 137–144. [CrossRef]
- 114. Fu, R.; Tang, S.; Lu, J.; Cui, Y.; Li, Z.; Zhang, H.; Xu, T.; Chen, Z.; Liu, C. Hot-wire arc additive manufacturing of aluminum alloy with reduced porosity and high deposition rate. *Mater. Des.* **2021**, *199*, 199109370. [CrossRef]
- 115. Zhang, C.; Li, Y.; Gao, M.; Zeng, X. Wire arc additive manufacturing of Al-6Mg alloy using variable polarity cold metal transfer arc as power source. *Mater. Sci. Eng. A* **2018**, 711, 415–423. [CrossRef]
- 116. Corbin, D.J.; Nassar, A.R.; Reutzel, E.W.; Kistler, N.A.; Beese, A.M.; Michaleris, P. Impact of directed energy deposition parameters on mechanical distortion of laser deposited Ti-6Al-4V. In Proceedings of the 27th Annual International Solid Freeform Fabrication Symposium—An Additive Manufacturing Conference SFF, Austin, TX, USA, 8–10 August 2016; pp. 670–679.
- 117. Xiong, J.; Lei, Y.; Li, R. Finite element analysis and experimental validation of thermal behavior for thin-walled parts in GMAW-based additive manufacturing with various substrate preheating temperatures. *Appl. Therm. Eng.* **2017**, 126, 43–52. [CrossRef]

118. Zhao, J.; Quan, G.Z.; Zhang, Y.Q.; Ma, Y.Y.; Jiang, L.H.; Dai, W.W.; Jiang, Q. Influence of deposition path strategy on residual stress and deformation in weaving wire-arc additive manufacturing of disc parts. *J. Mater. Res. Technol.* **2024**, *30*, 2242–2256. [CrossRef]

- 119. Ouellet, T.; Croteau, M.; Bois-Brochu, A.; Lévesque, J. Wire Arc Additive Manufacturing of Aluminium Alloys. *Eng. Proc.* **2023**, 43, 16. [CrossRef]
- 120. Zhang, J.; Wang, X.; Paddea, S.; Zhang, X. Fatigue crack propagation behaviour in wire+arc additive manufactured Ti-6Al-4V: Effects of microstructure and residual stress. *Mater. Des.* **2016**, *90*, 551–561. [CrossRef]
- 121. Gu, J.; Gao, M.; Yang, S.; Bai, J.; Zhai, Y.; Ding, J. Microstructure, defects, and mechanical properties of wire + arc additively manufactured Al[sbnd]Cu4.3-Mg1.5 alloy. *Mater. Des.* **2020**, *186*, 108357. [CrossRef]
- 122. Kindermann, R.M.; Roy, M.J.; Morana, R.; Francis, J.A. Effects of microstructural heterogeneity and structural defects on the mechanical behaviour of wire + arc additively manufactured Inconel 718 components. *Mater. Sci. Eng. A* 2022, 839, 142826. [CrossRef]
- 123. Yildiz, A.S.; Koc, B.I.; Yilmaz, O. Thermal behavior determination for wire arc additive manufacturing process. *Procedia Manuf.* **2020**, *54*, 233–237. [CrossRef]
- 124. Pawlik, J.; Cieślik, J.; Bembenek, M.; Góral, T.; Kapayeva, S.; Kapkenova, M. On the Influence of Linear Energy/Heat Input Coefficient on Hardness and Weld Bead Geometry in Chromium-Rich Stringer GMAW Coatings. *Materials* **2022**, *15*, 6019. [CrossRef]
- 125. Romanenko, D.; Prakash, V.J.; Kuhn, T.; Moeller, C.; Hintze, W.; Emmelmann, C. Effect of DED process parameters on distortion and residual stress state of additively manufactured Ti-6Al-4V components during machining. *Procedia CIRP* **2022**, *11*, 271–276. [CrossRef]
- 126. Mu, H.; Polden, J.; Li, Y.; He, F.; Xia, C.; Pan, Z. Layer-by-layer model-based adaptive control for wire arc additive manufacturing of thin-wall structures. *J. Intell. Manuf.* **2022**, 33, 1165–1180. [CrossRef]
- 127. Liu, B.; Lan, J.; Liu, H.; Chen, X.; Zhang, X.; Jiang, Z.; Han, J. The Effects of Processing Parameters during the Wire Arc Additive Manufacturing of 308L Stainless Steel on the Formation of a Thin-Walled Structure. *Materials* 2024, 17, 1337. [CrossRef] [PubMed]
- 128. Ali, M.H.; Han, Y.S. A Finite Element Analysis on the Effect of Scanning Pattern and Energy on Residual Stress and Deformation in Wire Arc Additive Manufacturing of EH36 Steel. *Materials* 2023, 16, 4698. [CrossRef] [PubMed]
- 129. Chen, S.; He, T.; Wu, X.; Lei, G. Synergistic effect of carbides and residual strain on the mechanical behavior of Ni-17 Mo-7Cr superalloy made by wire-arc additive manufacturing. *Mater Lett.* **2021**, 287, 129291. [CrossRef]
- 130. Winczek, J.; Gucwa, M.; Makles, K.; Mičian, M.; Yadav, A. The amount of heat input to the weld per unit length and per unit volume. *IOP Conf. Ser. Mater. Sci. Eng.* **2021**, *1199*, 012067. [CrossRef]
- 131. Koli, Y.; Arora, S.; Ahmad, S.; Priya Yuvaraj, N.; Khan, Z.A. Investigations and Multi-response Optimization of Wire Arc Additive Manufacturing Cold Metal Transfer Process Parameters for Fabrication of SS308L Samples. *J. Mater. Eng. Perform.* **2023**, *32*, 2463–2475. [CrossRef]
- 132. Cambon, C.; Rouquette, S.; Bendaoud, I.; Bordreuil, C.; Wimpory, R.; Soulie, F. Thermo-mechanical simulation of overlaid layers made with wire + arc additive manufacturing and GMAW-cold metal transfer. *Weld World* **2020**, *64*, 1427–1435. [CrossRef]
- 133. Omiyale, B.O.; Olugbade, T.O.; Abioye, T.E.; Farayibi, P.K. Wire arc additive manufacturing of aluminium alloys for aerospace and automotive applications: A review. *Mater. Sci. Technol.* **2022**, *38*, 391–408. [CrossRef]
- 134. Wang, J.; Pan, Z.; Carpenter, K.; Han, J.; Wang, Z.; Li, H. Comparative study on crystallographic orientation, precipitation, phase transformation and mechanical response of Ni-rich NiTi alloy fabricated by WAAM at elevated substrate heating temperatures. *Mater. Sci. Eng. A* **2021**, *800*, 140307. [CrossRef]
- 135. Ding, J.; Colegrove, P.; Martina, F.; Williams, S.; Wiktorowicz, R.; Palt, M.R. Development of a laminar flow local shielding device for wire + arc additive manufacture. *J. Mater. Process. Technol.* **2015**, 226, 99–105. [CrossRef]
- 136. Tonelli, L.; Laghi, V.; Palermo, M.; Trombetti, T.; Ceschini, L. AA5083 (Al–Mg) plates produced by wire-and-arc additive manufacturing: Effect of specimen orientation on microstructure and tensile properties. *Prog. Addit. Manuf.* **2021**, *6*, 479–494. [CrossRef]
- 137. Zhang, C.; Shen, C.; Hua, X.; Li, F.; Zhang, Y.; Zhu, Y. Influence of wire-arc additive manufacturing path planning strategy on the residual stress status in one single buildup layer. *Int. J. Adv. Manuf. Technol.* **2020**, *111*, 797–806. [CrossRef]
- 138. Denlinger, E.R.; Heigel, J.C.; Michaleris, P.; Palmer, T.A. Effect of inter-layer dwell time on distortion and residual stress in additive manufacturing of titanium and nickel alloys. *J. Mater. Process. Technol.* **2015**, 215, 123–131. [CrossRef]
- 139. Gudur, S.; Nagallapati, V.; Pawar, S.; Muvvala, G.; Simhambhatla, S. A study on the effect of substrate heating and cooling on bead geometry in wire arc additive manufacturing and its correlation with cooling rate. *Mater. Today Proc.* **2019**, *41*, 431–436. [CrossRef]
- 140. Singh, S.; Jinoop, A.N.; Tarun Kumar, G.T.A.; Palani, I.A.; Paul, C.P.; Prashanth, K.G. Effect of interlayer delay on the microstructure and mechanical properties of wire arc additive manufactured wall structures. *Materials* **2021**, *14*, 4187. [CrossRef] [PubMed]
- 141. Bermingham, M.J.; Nicastro, L.; Kent, D.; Chen, Y.; Dargusch, M.S. Optimising the mechanical properties of Ti-6Al-4V components produced by wire + arc additive manufacturing with post-process heat treatments. *J. Alloys Compd.* **2018**, 753, 247–255. [CrossRef]
- 142. Kumar, A.; Maji, K. Selection of Process Parameters for Near-Net Shape Deposition in Wire Arc Additive Manufacturing by Genetic Algorithm. *J. Mater. Eng. Perform.* **2020**, 29, 3334–3352. [CrossRef]
- 143. Ali, Y.; Henckell, P.; Hildebrand, J.; Reimann, J.; Bergmann, J.P.; Barnikol-Oettler, S. Wire arc additive manufacturing of hot work tool steel with CMT process. *J. Mater. Process. Technol.* **2019**, 269, 109–116. [CrossRef]

144. Laghi, V.; Palermo, M.; Tonelli, L.; Gasparini, G.; Ceschini, L.; Trombetti, T. Tensile properties and microstructural features of 304L austenitic stainless steel produced by wire-and-arc additive manufacturing. *Int. J. Adv. Manuf. Technol.* **2020**, *106*, 3693–3705. [CrossRef]

- 145. Dinovitzer, M.; Chen, X.; Laliberte, J.; Huang, X.; Frei, H. Effect of wire and arc additive manufacturing (WAAM) process parameters on bead geometry and microstructure. *Addit. Manuf.* **2019**, *26*, 138–146. [CrossRef]
- 146. Naveen Srinivas, M.; Vimal, K.E.K.; Manikandan, N.; Sritharanandh, G. Parametric optimization and multiple regression modelling for fabrication of aluminium alloy thin plate using wire arc additive manufacturing. *Int. J. Interact. Des. Manuf.* 2022. [CrossRef]
- 147. Zavdoveev, A.; Pozniakov, V.; Baudin, T.; Kim, H.S.; Klochkov, I.; Motrunich, S.; Heaton, M.; Aquier, P.; Rogante, M.; Denisenko, A.; et al. Optimization of the pulsed arc welding parameters for wire arc additive manufacturing in austenitic steel applications. *Int. J. Adv. Manuf. Technol.* **2022**, *119*, 5175–5193. [CrossRef]
- 148. Lu, X.; Li, M.V.; Yang, H. Comparison of wire-arc and powder-laser additive manufacturing for IN718 superalloy: Unified consideration for selecting process parameters based on volumetric energy density. *Int. J. Adv. Manuf. Technol.* **2021**, 114, 1517–1531. [CrossRef]
- 149. Vora, J.; Pandey, R.; Dodiya, P.; Patel, V.; Khanna, S.; Vaghasia, V.; Chaudhari, R. Fabrication of Multi-Walled Structure through Parametric Study of Bead Geometries of GMAW-Based WAAM Process of SS309L. *Materials* 2023, 16, 5147. [CrossRef] [PubMed]
- 150. Athaib, N.H.; Haleem, A.H.; Al-Zubaidy, B. A review of Wire Arc Additive Manufacturing (WAAM) of Aluminium Composite, Process, Classification, Advantages, Challenges, and Application. *J. Phys. Conf. Ser.* **2021**, 1973, 012083. [CrossRef]
- 151. Scharf-Wildenhain, R.; Haelsig, A.; Hensel, J.; Wandtke, K.; Schroepfer, D.; Kannengiesser, T. Heat control and design-related effects on the properties and welding stresses in WAAM components of high-strength structural steels. *Weld World* **2023**, *67*, 55–65. [CrossRef]
- 152. Zhang, J.; Zhang, X.; Wang, X.; Ding, J.; Traoré, Y.; Paddea, S.; Williams, S. Crack path selection at the interface of wrought and wire + arc additive manufactured Ti-6Al-4V. *Mater. Des.* **2016**, *104*, 365–375. [CrossRef]
- 153. Yang, Y.H.; Guan, Z.P.; Ma, P.K.; Ren, M.W.; Jia, H.L.; Zhao, P.; Zha, M.; Wang, H.Y. Wire arc additive manufacturing of a novel ATZM31 Mg alloy: Microstructure evolution and mechanical properties. *J. Magnes. Alloys* **2023**, *10*, 44. [CrossRef]
- 154. Koli, Y.; Yuvaraj, N.; Sivanandam, A.; Vipin. Control of humping phenomenon and analyzing mechanical properties of Al–Si wire-arc additive manufacturing fabricated samples using cold metal transfer process. *Proc. Inst. Mech. Eng. Part C J. Mech. Eng. Sci.* 2022, 236, 984–996. [CrossRef]
- 155. Jing, Y.; Fang, X.; Xi, N.; Chang, T.; Duan, Y.; Huang, K. Improved tensile strength and fatigue properties of wire-arc additively manufactured 2319 aluminum alloy by surface laser shock peening. *Mater. Sci. Eng. A* **2023**, *864*, 144599. [CrossRef]
- 156. Chi, J.; Cai, Z.; Wan, Z.; Zhang, H.; Chen, Z.; Li, L.; Li, Y.; Peng, P.; Guo, W. Effects of heat treatment combined with laser shock peening on wire and arc additive manufactured Ti17 titanium alloy: Microstructures, residual stress and mechanical properties. *Surf. Coat. Technol.* **2020**, *396*, 125908. [CrossRef]
- 157. Sousa, B.M.; Coelho, F.G.F.; Júnior, G.M.M.; de Oliveira, H.C.P.; da Silva, N.N. Thermal and microstructural analysis of intersections manufactured by wire arc additive manufacturing (WAAM). *Weld World* **2024**, *68*, 1653–1669. [CrossRef]
- 158. Ma, D.; Xu, C.; Sui, S.; Tian, J.; Guo, C.; Wu, X.; Zhang, Z.; Remennik, S.; Shechtman, D. Microstructure evolution and mechanical properties of wire arc additively manufactured Mg-Gd-Y-Zr alloy by post heat treatments. *Virtual Phys. Prototyp.* **2023**, *18*, 1–22. [CrossRef]
- 159. Szost, B.A.; Terzi, S.; Martina, F.; Boisselier, D.; Prytuliak, A.; Pirling, T.; Hofmann, M.; Jarvis, D.J. A comparative study of additive manufacturing techniques: Residual stress and microstructural analysis of CLAD and WAAM printed Ti-6Al-4V components. *Mater. Des.* **2016**, *89*, 559–567. [CrossRef]
- 160. Kumar, A.; Maji, K.; Shrivastava, A. Investigations on Deposition Geometry and Mechanical Properties of Wire Arc Additive Manufactured Inconel 625. *Int. J. Precis. Eng. Manuf.* **2023**, 24, 1483–1500. [CrossRef]
- 161. Vazquez, L.; Rodriguez, M.N.; Rodriguez, I.; Alvarez, P. Influence of post-deposition heat treatments on the microstructure and tensile properties of ti-6al-4v parts manufactured by cmt-waam. *Metals* **2021**, *11*, 1161. [CrossRef]
- 162. Geng, H.; Li, J.; Xiong, J.; Lin, X.; Zhang, F. Optimization of wire feed for GTAW based additive manufacturing. *J. Mater. Process. Technol.* **2017**, 243, 40–47. [CrossRef]
- 163. Li, R.; Xiong, J.; Lei, Y. Investigation on thermal stress evolution induced by wire and arc additive manufacturing for circular thin-walled parts. *J. Manuf. Process.* **2019**, *40*, 59–67. [CrossRef]
- 164. Gupta, N.K.; Ganesan, G.B.; Karade, S.; Mehta, A.K.; Karunakaran, K.P. Effect of Multiple Technologies on Minimizing the Residual Stresses in Additive Manufacturing. In Proceedings of the ICRS 11—The 11th International Conference of Residual Stresses, Nancy, France, 27–30 March 2022; p. 040150.
- 165. Ali, M.H.; Han, Y.S. Effect of phase transformations on scanning strategy in waam fabrication. *Materials* **2021**, *14*, 7871. [CrossRef] [PubMed]
- 166. Gornyakov, V.; Sun, Y.; Ding, J.; Williams, S. Modelling and optimising hybrid process of wire arc additive manufacturing and high-pressure rolling. *Mater. Des.* **2022**, 223, 111121. [CrossRef]
- 167. Gornyakov, V. Efficient Modelling and Evaluation of Rolling for Mitigation of Residual Stress and Distortion in Wire Arc Additive Manufacturing. Ph.D. Thesis, Cranfield University, Cranfield, UK, 2021. Volume 7. p. 265.

168. Zhang, T.; Li, H.; Gong, H.; Ding, J.; Wu, Y.; Diao, C.; Zhang, X.; Williams, S. Hybrid wire-arc additive manufacture and effect of rolling process on microstructure and tensile properties of Inconel 718. *J. Mater. Process. Technol.* **2022**, 299, 321–326. [CrossRef]

- 169. Srivastava, S.; Garg, R.K.; Sharma, V.S.; Sachdeva, A. Measurement and Mitigation of Residual Stress in Wire-Arc Additive Manufacturing: A Review of Macro-Scale Continuum Modelling Approach. *Arch. Comput. Methods Eng.* **2021**, 28, 3491–3515. [CrossRef]
- 170. Montevecchi, F.; Venturini, G.; Scippa, A.; Campatelli, G. Finite Element Modelling of Wire-arc-additive-manufacturing Process. *Procedia CIRP* **2016**, *55*, 109–114. [CrossRef]
- 171. Bankong, B.D.; Abioye, T.E.; Olugbade, T.O.; Zuhailawati, H.; Gbadeyan, O.O.; Ogedengbe, T.I. Review of post-processing methods for high-quality wire arc additive manufacturing. *Mater. Sci. Technol.* **2023**, *39*, 129–146. [CrossRef]
- 172. Hönnige, J.R.; Colegrove, P.A.; Ahmad, B.; Fitzpatrick, M.E.; Ganguly, S.; Lee, T.L.; Williams, S.W. Residual stress and texture control in Ti-6Al-4V wire + arc additively manufactured intersections by stress relief and rolling. *Mater. Des.* **2018**, *150*, 193–205. [CrossRef]
- 173. Li, K.; Klecka, M.A.; Chen, S.; Xiong, W. Wire-arc additive manufacturing and post-heat treatment optimization on microstructure and mechanical properties of Grade 91 steel. *Addit. Manuf.* **2021**, *37*, 101734. [CrossRef]
- 174. Nie, L.; Wu, Y.; Gong, H.; Chen, D.; Guo, X. Effect of shot peening on redistribution of residual stress field in friction stir welding of 2219 aluminum alloy. *Materials* **2020**, *13*, 3169. [CrossRef]
- 175. Sun, R.; Li, L.; Zhu, Y.; Guo, W.; Peng, P.; Cong, B.; Sun, J.; Che, Z.; Li, B.; Guo, C.; et al. Microstructure, residual stress and tensile properties control of wire-arc additive manufactured 2319 aluminum alloy with laser shock peening. *J. Alloys Compd.* **2018**, 747, 255–265. [CrossRef]
- 176. Ermakova, A.; Razavi, N.; Cabeza, S.; Gadalinska, E.; Reid, M.; Paradowska, A.; Ganguly, S.; Berto, F.; Mehmanparast, A. The effect of surface treatment and orientation on fatigue crack growth rate and residual stress distribution of wire arc additively manufactured low carbon steel components. *J. Mater. Res. Technol.* 2023, 24, 2988–3004. [CrossRef]
- 177. Ding, Y.; Muñiz-Lerma, J.A.; Trask, M.; Chou, S.; Walker, A.; Brochu, M. Microstructure and mechanical property considerations in additive manufacturing of aluminum alloys. *MRS Bull.* **2016**, *41*, 745–751. [CrossRef]
- 178. Busachi, A.; Erkoyuncu, J.; Colegrove, P.; Martina, F.; Ding, J. Designing a WAAM based manufacturing system for defence applications. *Procedia CIRP* **2015**, *37*, 48–53. [CrossRef]
- 179. Abusalma, H.; Eisazadeh, H.; Hejripour, F.; Bunn, J.; Aidun, D. Parametric study of residual stress formation in Wire and Arc Additive Manufacturing. *J. Manuf. Process.* **2022**, *75*, 863–876. [CrossRef]
- 180. Kyvelou, P.; Huang, C.; Li, J.; Gardner, L. Residual stresses in steel I-sections strengthened by wire arc additive manufacturing. In *Structures*; Elsevier: Amsterdam, The Netherlands, 2024; Volume 60.
- 181. Wu, B.; Pan, Z.; Ding, D.; Cuiuri, D.; Li, H.; Xu, J.; Norrish, J. A review of the wire arc additive manufacturing of metals: Properties, defects and quality improvement. *J. Manuf. Process.* **2018**, *35*, 127–139. [CrossRef]
- 182. Colegrove, P.A.; Donoghue, J.; Martina, F.; Gu, J.; Prangnell, P.; Hönnige, J. Application of bulk deformation methods for microstructural and material property improvement and residual stress and distortion control in additively manufactured components. *Scr. Mater.* **2017**, *135*, 111–118. [CrossRef]
- 183. Karmuhilan, M.; Sood, A.K. Intelligent process model for bead geometry prediction in WAAM. *Mater. Today Proc.* **2018**, *5*, 24005–24013. [CrossRef]
- 184. Tang, S.; Wang, G.; Huang, C.; Li, R.; Zhou, S.; Zhang, H. Investigation, modeling and optimization of abnormal areas of weld beads in wire and arc additive manufacturing. *Rapid Prototyp J.* **2020**, *26*, 183–195. [CrossRef]
- 185. Veiga, F.; Suárez, A.; Aldalur, E.; Bhujangrao, T. Effect of the metal transfer mode on the symmetry of bead geometry in waam aluminum. *Symmetry* **2021**, *13*, 1245. [CrossRef]
- 186. Ding, D.; Pan, Z.; Cuiuri, D.; Li, H. A multi-bead overlapping model for robotic wire and arc additive manufacturing (WAAM). *Robot Comput. Integr. Manuf.* **2015**, *31*, 101–110. [CrossRef]
- 187. Geng, H.; Xiong, J.; Huang, D.; Lin, X.; Li, J. A prediction model of layer geometrical size in wire and arc additive manufacture using response surface methodology. *Int. J. Adv. Manuf. Technol.* **2017**, *93*, 175–186. [CrossRef]
- 188. Banaee, S.A.; Kapil, A.; Marefat, F.; Sharma, A. Generalised overlapping model for multi-material wire arc additive manufacturing (WAAM). *Virtual Phys. Prototyp.* **2023**, *18*, e2210541. [CrossRef]
- 189. Surovi, N.A.; Soh, G.S. Acoustic feature based geometric defect identification in wire arc additive manufacturing. *Virtual Phys. Prototyp.* **2023**, *18*, e2210553. [CrossRef]
- 190. Zhao, Y.T.; Li, W.G.; Liu, A. Optimization of geometry quality model for wire and arc additive manufacture based on adaptive multi-objective grey wolf algorithm. *Soft Comput.* **2020**, *24*, 17401–17416. [CrossRef]
- 191. Alomari, Y.; Birosz, M.T.; Andó, M. Part orientation optimization for Wire and Arc Additive Manufacturing process for convex and non-convex shapes. *Sci. Rep.* **2023**, *13*, 2203. [CrossRef] [PubMed]
- 192. Wani, Z.K.; Abdullah, A.B. Bead Geometry Control in Wire Arc Additive Manufactured Profile—A Review. *Pertanika J. Sci. Technol.* **2024**, 32, 917–942. [CrossRef]
- 193. Vora, J.; Parikh, N.; Chaudhari, R.; Patel, V.K.; Paramar, H.; Pimenov, D.Y.; Giasin, K. Optimization of bead morphology for GMAW-based wire-arc of 2.25 Cr-1.0 Mo steel using metal-cored wires. *Appl. Sci.* **2022**, *12*, 5060. [CrossRef]
- 194. Wang, C.; Bai, H.; Ren, C.; Fang, X.; Lu, B. A comprehensive prediction model of bead geometry in wire and arc additive manufacturing. *J. Phys. Conf. Ser.* **2020**, *1624*, 022018. [CrossRef]

195. Chintala, A.; Tejaswi Kumar, M.; Sathishkumar, M.; Arivazhagan, N.; Manikandan, M. Technology Development for Producing Inconel 625 in Aerospace Application Using Wire Arc Additive Manufacturing Process. *J. Mater. Eng. Perform.* **2021**, *30*, 5333–5341. [CrossRef]

- 196. Hamrani, A.; Bouarab, F.Z.; Agarwal, A.; Ju, K.; Akbarzadeh, H. Advancements and applications of multiple wire processes in additive manufacturing: A comprehensive systematic review. *Virtual Phys. Prototyp.* **2023**, *18*, e2273303. [CrossRef]
- 197. Queguineur, A.; Rückert, G.; Cortial, F.; Hascoët, J.Y. Evaluation of wire arc additive manufacturing for large-sized components in naval applications. *Weld World* **2018**, *62*, 259–266. [CrossRef]
- 198. Li, J.; Cui, Q.; Pang, C.; Xu, P.; Luo, W.; Li, J. Integrated vehicle chassis fabricated by wire and arc additive manufacturing: Structure generation, printing radian optimisation, and performance prediction. *Virtual Phys. Prototyp.* **2024**, *19*, e2301483. [CrossRef]
- 199. Singh, S.R.; Khanna, P. Wire arc additive manufacturing (WAAM): A new process to shape engineering materials. *Mater. Today Proc.* **2021**, *44*, 118–128. [CrossRef]
- 200. Vishnukumar, M.; Pramod, R.; Rajesh Kannan, A. Wire arc additive manufacturing for repairing aluminium structures in marine applications. *Mater. Lett.* **2021**, 299, 130112. [CrossRef]
- 201. Shah, A.; Aliyev, R.; Zeidler, H.; Krinke, S. A Review of the Recent Developments and Challenges in Wire Arc Additive Manufacturing (WAAM) Process. *J. Manuf. Mater. Process.* **2023**, *7*, 97. [CrossRef]
- 202. Chaturvedi, M.; Scutelnicu, E.; Rusu, C.C.; Mistodie, L.R.; Mihailescu, D.; Subbiah, A.V. Wire Arc Additive Manufacturing: Review on Recent Findings and Challenges in Industrial Applications and Materials Characterization. *Metals* **2021**, *11*, 939. [CrossRef]
- 203. Boţilă, L.N. Considerations regarding aluminum alloys used in the aeronautic/aerospace industry and use of wire arc additive manufacturing WAAM for their industrial applications. *Test* **2020**, *4*, 9–24.
- 204. Liu, J.; Xu, Y.; Ge, Y.; Hou, Z.; Chen, S. Wire and arc additive manufacturing of metal components: A review of recent research developments. *Int. J. Adv. Manuf. Technol.* **2020**, *111*, 149–198. [CrossRef]
- 205. Arana, M.; Ukar, E.; Rodriguez, I.; Aguilar, D.; Álvarez, P. Influence of deposition strategy and heat treatment on mechanical properties and microstructure of 2319 aluminium WAAM components. *Mater. Des.* **2022**, 221, 110974. [CrossRef]
- 206. Thapliyal, S. Challenges associated with the wire arc additive manufacturing (WAAM) of Aluminum alloys. *Mater. Today Proc.* **2019**, 221, 112006. [CrossRef]
- 207. Zhao, Y.; Li, F.; Chen, S.; Lu, Z. Unit block–based process planning strategy of WAAM for complex shell–shaped component. *Int. J. Adv. Manuf. Technol.* **2019**, 104, 3915–3927. [CrossRef]
- 208. Pant, H.; Arora, A.; Gopakumar, G.S.; Chadha, U.; Saeidi, A.; Patterson, A.E. Applications of wire arc additive manufacturing (WAAM) for aerospace component manufacturing. *Int. J. Adv. Manuf. Technol.* **2023**, 127, 4995–5011. [CrossRef]
- 209. Bachus, N.A.; Strantza, M.; Clausen, B.; D'Elia, C.R.; Hill, M.R.; Ko, J.P.; Pagan, D.C.; Brown, D.W. Novel bulk triaxial residual stress mapping in an additive manufactured bridge sample by coupling energy dispersive X-ray diffraction and contour method measurements. *Addit. Manuf.* 2024, *83*, 104070. [CrossRef]
- 210. Gordon, J.V.; Haden, C.V.; Nied, H.F.; Vinci, R.P.; Harlow, D.G. Fatigue crack growth anisotropy, texture and residual stress in austenitic steel made by wire and arc additive manufacturing. *Mater. Sci. Eng. A* **2018**, *115*, 60–66. [CrossRef]

Disclaimer/Publisher's Note: The statements, opinions and data contained in all publications are solely those of the individual author(s) and contributor(s) and not of MDPI and/or the editor(s). MDPI and/or the editor(s) disclaim responsibility for any injury to people or property resulting from any ideas, methods, instructions or products referred to in the content.